Polymerization of Olefins Through Heterogeneous Catalysis. XVIII. A Kinetic Explanation for Unusual Effects

W. K. ALEX SHAFFER, W. HARMON RAY

University of Wisconsin, Chemical Engineering Department, Madison, Wisconsin 53706

Received 5 September 1996; accepted 12 September 1996

ABSTRACT: The development of a detailed kinetic model describing some of the unusual effects observed in catalyzed olefin polymerization is presented. Based on the method of moments, the model describes the rate effects of hydrogen and comonomers, as well as the ability of certain systems to incorporate long chain branches via internal and/or terminal double bond polymerization. Examples are provided demonstrating the model's ability to predict rates and degrees of polymerization with ethylene, propylene, and 1-hexene monomers. In the case of propylene, multiple insertion mechanisms are modeled and compared with experimental sequence length and end group data. In other examples the model is used to simulate an oscillating metallocene catalyst and a metallocene catalyst capable of branch addition via terminal double bond polymerization. © 1997 John Wiley & Sons, Inc. J Appl Polym Sci **65:** 1053–1080, 1997

Key words: olefin polymerization; kinetics; polymer properties; modeling

INTRODUCTION

Ziegler–Natta catalysis has significantly advanced since its introduction nearly 50 years ago. In fact, from the vantage point of the outsider, such catalyzed polyolefin processes appear to be mature technologies based on well understood chemical phenomena. While this view is not entirely inappropriate with regard to many of the overall technologies currently in use, it is somewhat illusory from the standpoint of how well the underlying chemistry is understood. The outsider, for instance, would reasonably expect that in such a multimillion ton business that there is a good understanding of the basic reaction mechanisms and kinetics. In reality, however, the literature contains a myriad of proposals which are further complicated by variations in the physical state of the catalyst, catalyst oxidation state, addition of donors, etc. Even the stereoregulating ability of Ziegler–Natta catalysts, clearly one of the most important features of these systems, is not completely understood at the fundamental chain building level. Moreover, with companies spending millions of dollars to develop a new generation of transition metal catalysts, the so-called metallocenes, the need to understand these systems is greater than ever.

This article focuses on modeling the kinetics of catalyzed olefin polymerization with the idea that there are basic mechanisms at work which are independent of the almost infinite number of possible combinations of catalyst types and chemical environments. In carrying out this investigation, it is first useful to consider the generally accepted mechanisms which may be found throughout the literature. Chen[1] has consolidated much of this information to arrive at the set of equations and rate expressions presented in Table I.

According to the standard kinetic scheme in Table I, potential sites (C_{pot}) of the catalyst must undergo activation by species A (e.g., alkyl cocatalyst, electron donor, hydrogen, or monomer) or spontaneously to create vacant sites (P_0^k) of type k. Chain building then begins with initiation to

Correspondence to: W. Harmon Ray.

 CCC 0021-8995/97/061053-28

Table I Standard Catalyzed Olefin Polymerization Mechanisms

Activation	$C_{pot} + A \rightarrow P_o^k$	$R_{aA}^k = k_{aA}^k C_{pot} C_{A,eff}^{O_{aA}^k}$
	$C_{pot} \rightarrow P_o^k$	$R_{aSp}^k = k_{aSp}^k C_{pot}^{O_{aSp}^k}$
Initiation	$P_o^k + M_i \rightarrow P_{\underline{\delta}_i,i}^k$	$R_{pi}^k = k_{pi}^k P_o^k C_{M_i,eff}$
Propagation	$P_{\underline{n},j}^k + M_i \rightarrow P_{\underline{n}+\underline{\delta}_i,i}^k$	$R_{pij}^k = k_{pij}^k P_{\underline{n},j}^k C_{M_i,eff}$
Chain Transfer	$P_{\underline{n},j}^k + T \rightarrow P_o^k + D_{\underline{n},j}^k$	$R_{cTj}^k = k_{cTj}^k P_{\underline{n},j}^k C_{T,eff}^{O_{cTj}^k}$
	$P_{\underline{n},j}^k + M_i \rightarrow P_{\underline{\delta}_i,i}^k + D_{\underline{n},j}^k$	$R_{cM_ij}^k = k_{cM_ij}^k P_{\underline{n},j}^k C_{M_i,eff}^{O_{cM_ij}^k}$
	$P_{\underline{n},j}^k \rightarrow P_o^k + D_{\underline{n},j}^k$	$R_{cSpj}^k = k_{cSpj}^k P_{\underline{n},j}^k$
Site Transformation	$P_o^k + X \rightarrow P_o^l$	$R_{tL}^{kl} = k_{tL}^{kl}(P_o^k + P_{\underline{n},j}^k) C_{X,eff}^{O_{tL}^{kl}}$
	$P_{\underline{n},j}^k + X \rightarrow P_o^l + D_{\underline{n},j}^k$	
	$P_o^k \rightarrow P_o^l$	$R_{tSp}^{kl} = k_{tSp}^{kl}(P_o^k + P_{\underline{n},j}^k)$
	$P_{\underline{n},j}^k \rightarrow P_o^l + D_{\underline{n},j}^k$	
Deactivation	$P_o^k + X \rightarrow C_d$	$R_{dX}^k = k_{dX}^k(P_o^k + P_{\underline{n},j}^k) C_{X,eff}^{O_{dX}^k}$
	$P_{\underline{n},j}^k + X \rightarrow C_d + D_{\underline{n},j}^k$	
	$P_o^k \rightarrow C_d$	$R_{dSp}^k = k_{dSp}^k(P_o^k + P_{\underline{n},j}^k)$
	$P_{\underline{n},j}^k \rightarrow C_d + D_{\underline{n},j}^k$	

form a chain of length one ($P_{\delta_i,i}^k$), followed by rapid propagation to generate chains ($P_{n,j}^k$) having composition n (i.e., n_1 = amount of monomer 1, n_2 = amount of monomer 2, etc.) and end group j. Polymer molecular weight is controlled by spontaneous chain transfer or chain transfer with agent T (e.g., transfer agent, hydrogen, alkyl cocatalyst, electron donor, or solvent) to create a dead polymer chain ($D_{n,j}^k$) and a vacant active site. Chain transfer may also occur due to reaction with the monomer itself; however, such reaction leads to the formation of a live polymer chain of length unity. Finally, the mechanisms of site transformation and deactivation may occur spontaneously or by reaction with species X (e.g., poison, hydrogen, alkyl cocatalyst, electron donor, solvent, or monomer). The former mechanism transforms sites of one type k to another type l, while the latter mechanism creates permanently deactivated sites (C_d). In both cases the growing polymer chain is terminated.

In the sections of this article which follow, shortcomings of the current model are discussed and improvements are suggested. Applying the method of moments, these improvements are then incorporated into the model and demonstrated with examples using the POLYRED™ simulation package.[2]

SHORTCOMINGS IN THE KINETIC MODEL

Although useful, the kinetic scheme presented in Table I is unable to describe several commonly observed phenomena. Of primary interest are the rate effects observed when polymerizing olefins in the presence of hydrogen or comonomer, as well as the ability of certain systems to incorporate long chain branches. In the subsections that follow, these and other shortcomings of the kinetic scheme in Table I are discussed. In some cases only modifications are required, while in others, entirely new reactions must be added to model these phenomena.

Hydrogen Rate Effects

Natta et al.[3] were among the first to study the effects of hydrogen on catalyzed olefin polymerizations. They performed both ethylene and propylene polymerizations with the $AlEt_3$/alpha-$TiCl_3$ catalyst system to observe the effect of hydrogen on molecular weight, isotacticity, and polymerization rate. In the case of molecular weight, they found that the experimental data for both ethylene and propylene were fit well using eq. (2), which is similar in form to the Langmuir isotherm for dissociative adsorption.

$$\bar{M}_r = 1/(K_1 + K_2\sqrt{P_{H_2}}) \qquad (2)$$

They proposed that chain termination eq. (3) and subsequent reinitiation eq. (4) could be represented by the following two reactions where $[CAT]$ represents the active catalyst site, P_n is the live polymer chain, D_n is the dead polymer chain, and R is the monomer's hydrocarbon tail, if present.

$$[CAT] - P_n + H_2 \rightarrow [CAT] - H + D_n \quad (3)$$

$$[CAT] - H + RCH = CH_2 \rightarrow [CAT] - CH_2CH_2R \quad (4)$$

Based on this simple scheme, Natta attributed the observed rate decreases in the presence of hydrogen to slow reactivation of the $[CAT]$-H bond and demonstrated that the effect could be reversed by simply removing the hydrogen.

While studies by several independent researchers confirmed Natta's findings, there were also numerous investigations that yielded contradictory results. For example, the results of Hoffman, Fries, and Condit[4] using a tritium tracer for hydrogen in the polymerizations of propylene and 4-methyl-1-pentene with the $AlEt_2Cl/TiCl_3$ system, indicated the presence of two tracer hydrogens per polymer molecule, thus supporting Natta's conclusion that the $[CAT]$-H centers may be reactivated for further polymerization. On the other hand, Bourat, Ferrier, and Perez[5] obtained only one tracer hydrogen per polymer molecule when polymerizing propylene with the $AlEtCl_2/TiCl_3$ system, indicating that the $[CAT]$-H sites were incapable of further polymerization. Furthermore, to make matters more complex, researchers[6,7] using the gamma and delta forms of the $TiCl_3/AlCl_3$ catalyst system discovered that, in complete contrast to Natta's observations with the alpha form, hydrogen actually enhanced the catalyst activity for propylene polymerization.

Although the direction and magnitude of the hydrogen effect varies from one catalyst/donor/monomer system to another, the bulk of experimental data using today's higher activity $TiCl_4$ catalysts shows that hydrogen generally reduces the polymerization rate of ethylene and enhances the rate for propylene. In the case of propylene, for example, Guastalla and Giannini[8] observed that initial rates increased dramatically to their maximum with increasing hydrogen partial pressure, indicating that the activation process is very fast. In addition, they found that the initial rates increased asymptotically with hydrogen, indicating some sort of adsorption phenomena of hydrogen at the catalyst surface.

While some researchers believe that hydrogen rate enhancement may be due to improved monomer access at the active sites via increased chain migration[9] or reduced competition with terminal double bonds,[10] the results of Guastalla and Giannini suggest otherwise. In particular, propylene polymerizations performed at low temperatures

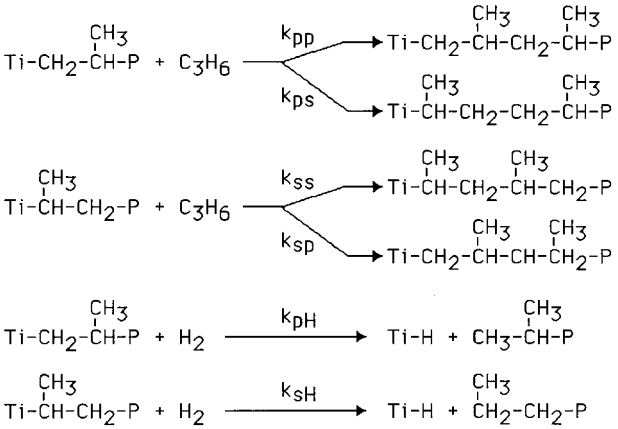

Figure 1 Propylene polyinsertion mechanism.

(17°C) did not raise catalyst activity, but still significantly decreased the polymer molecular weight. Thus Guastalla and Giannini concluded that the chain-regulating ability of hydrogen is not related to its activating influence. Furthermore, ethylene polymerizations with the same catalyst yielded decreasing activities as the hydrogen partial pressure was increased, indicating that stereospecificity might play some role.

Thanks to advances in polymer analysis techniques, much recent work has focused on the possible link between rate enhancement and the use of stereospecific monomers. Busico, Cipullo, and Corradini,[11] for example, investigated the polyinsertion of propylene over a highly isospecific $TiCl_4/MgCl_2$-supported catalyst using hydrogen as the chain transfer agent. As shown in Figure 1, propylene monomers may propagate via 1,2-insertion (k_{pp} or k_{sp}) and/or 2,1-insertion (k_{ps} or k_{ss}). Analysis of a typical gas chromatogram from such polymerizations revealed that each hydrooligomer with a given degree of polymerization ($X_n \leq 15$) can be put into one of two categories: one containing all possible diastereoisomers from a regioregular 1,2-insertion mechanism, and the other containing all possible diastereoisomers created by a 1,2-insertion mechanism with a 2,1-inserted terminal end.

The results for the species of each degree of polymerization showed that the ratio between 1,2- and 2,1-terminated hydrooligomers (Q_p/Q_s) was $\sim$ 6.4, 8.4, 12.0, and 13.4 for samples having average degrees of polymerization of 590, 320, 140, and 130, respectively. Assuming one active site type, chain termination exclusively with hydrogen, and steady-state conditions, Busico and coworkers obtained eq. (5)

$$Q_p/Q_s = (k_{sp}/k_{ps})(k_{pH}/k_{sH}) + (k_{pp}/k_{ps})/X_n(1 + Q_s/Q_p). \quad (5)$$

Using the GC measurements of Q_p/Q_s as a function of X_n, eq. (5) allows determination of the ratios of the kinetic constants for the given system: $k_{pp}/k_{ps} = 1.1 \pm 0.1*10^3$ and $(k_{sp}/k_{ps})(k_{pH}/k_{sH}) = 4.8 \pm 0.3$.

Supposing that the ratio k_{pH}/k_{sH} is of order unity (i.e., $0.5 \leq [k_{pH}/k_{sH}] \leq 2$) and defining τ to be the time required per 1,2-insertion, Busico and coworkers concluded that an occasional 2,1-insertion should take place approximately every $1.1*10^3\tau$. Furthermore, due to the low reactivity after 2,1-insertion, this step will be followed by a pause in chain growth on the order of $1*10^2\tau$ to $5*10^2\tau$ before 1,2-insertion continues. From this it then follows that each catalytic site is active $\sim 70-90\%$ of the time.

Such results suggest that chain transfer with hydrogen is more probable following 2,1-insertion due to the slowdown in growth at the sterically hindered site. Furthermore, these results are also supported by the end group analyses of Tsutsui, Kashiwa, and Mizuno,[12] as well as those of Chadwick, Miedema, and Sudmeijer.[13] Using a zirconium-based metallocene, the results of Tsutsui, Kashiwa, and Mizuno indicate that 2,1- and 1,3-terminated chains are essentially absent unless hydrogen is added to the polymerization. Similarly, the data of Chadwick, Miedema, and Sudmeijer reveal that the fraction of end groups formed by chain transfer following 2,1-insertion was the lowest for donors which gave the lowest hydrogen activation effect.

In modeling propylene polyinsertion and the corresponding hydrogen rate enhancement, it is necessary to reconsider the standard kinetic scheme in Table I. Firstly, the kinetic scheme must allow monomers to have multiple reactivities. The scheme in Table I can easily handle this by simply allowing for two reactive monomer groups (M_i) per monomer. Thus the balance on this particular monomer must account for disappearance due to reaction of either of these monomer groups. Secondly, the kinetic scheme must permit simultaneous chain transfer/site transformation so that a *CAT*-H site may be formed following chain transfer with hydrogen. This latter feature, however, is not present in the scheme of Table I, and must be added as shown in the more general kinetic scheme of Table VII.

In closing this discussion of hydrogen rate effects, it should be noted that various nonkinetic explanations for hydrogen rate enhancement have also been proposed. Parsons and Al-Turki,[14] for example, suggest that hydrogen might generate additional active centers via catalyst penetration resulting in subsequent separation of weakly adhering surfaces. They support this proposal with ^{14}CO radiotagging measurements that show a significant increase in the number of active sites upon addition of hydrogen. Chadwick, Miedema, and Sudmeijer,[13] however, believe that this apparent increase in active sites may be simply due to a relatively slow CO insertion at the less active 2,1-inserted sites. Furthermore, this mechanism is not consistent with the rate reduction observed in the case of ethylene.

Comonomer Rate Effects

Introducing comonomers means there will be competition with the primary monomer for insertion at the active centers. Although the resulting kinetics can frequently be predicted from the individual homopolymerization results, there are a number of cases where the resulting polymerization behavior is unpredictable and even counterintuitive.

An early study by Valvassori and coworkers[15] considered the kinetics of ethylene/propylene copolymerization using a vanadium catalyst. It was concluded at that time that the significant increase in the overall copolymerization rate observed with increasing the ethylene/propylene ratio could not be explained purely on the basis of the propagation rate constants. Rather, evidence was found suggesting that there is a variation in the total number of growing chains when changing the ethylene/propylene ratio. They proposed that this variation might be due to the presence of active centers that are able to start homopolymerization of ethylene, but not propylene. It is noted that this may be the case, for instance, if the addition rate of the first propylene monomer is much slower than the addition rate of subsequent units. By applying this approach, the authors were able to obtain an equation that fairly successfully explains the experimental values of the overall ethylene/propylene copolymerization rates.

Another study by Ivanchev and coworkers[16] considered ethylene/hexene-1 copolymerizations on $TiCl_4/MgCl_2$. They investigated the dependence of the copolymer hexene content (C_p) on the concentration of hexene in the reaction medium

(C_a) and found that the increase in C_p became less dramatic as C_a was increased from 0.1 to 0.5 mol/L. In addition, it was also discovered that increasing the polymerization temperature resulted in a reduction in C_p, contrary to the expected increase based on thermodynamic considerations. Ivanchev et al. believe this opposite trend indicates a change in the polymerization mechanism or in the structure of the active sites. They note that one possible change with increasing temperature is for the organoaluminum cocatalyst to reduce the oxidation state of the catalyst.

Although the rate of chain transfer was greater for hexene than ethylene, both M_n and M_w increased for the copolymerization. At the same time, the polydispersity M_w/M_n did not appear to depend on the concentration of hexene-1 since its value remained fairly constant. Ivanchev et al. interpreted these results as suggesting that the presence of comonomer leads to an activity increase of all growth centers rather than changing the distribution of active centers via structural heterogeneity. Thus they proposed a model of outer sphere complexing between the comonomer molecules and the catalyst active sites. According to this coordination model, the addition rates of monomer and comonomer into the polymer chain are determined by the effective concentrations close to the active sites rather than by activation energies for insertion into the metal–carbon bond. Such a model would also explain the decreasing copolymer content with increasing temperature, since at higher temperatures the number of comonomer molecules in the outer coordination sphere would be fewer.

More recently, Karol, Kao, and Cann[17] studied the phenomena of comonomer activation, noting that the effect is observed for many different catalysts (e.g., titanium, vanadium, chromium, and zirconium) under varying ligand environments. Thus they believe this comonomer effect to be a general characteristic common to many α-olefin copolymerization kinetics.

In searching for a mechanistic explanation, Karol, Kao, and Cann polymerized ethylene using high-activity titanium and vanadium catalysts. Initial studies revealed that the comonomer structure has a large effect on the resulting activity increase. Apparently the shorter the α-olefin, the greater the rate enhancement, that is, propylene $>$ 1-butene $>$ 1-hexene. In other experiments, dienes such as butadiene caused decreased activity, while internal olefins such as 2-hexene had no effect.

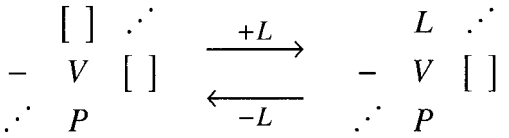

Figure 2 Reversible ligand coordination.

In the case of α-olefins, the observed effect is usually an initial rate acceleration followed by rapid decay. Catalyst deactivation is thought to be due to reaction of active sites with deactivating Lewis bases (including α-olefins) and/or to a decrease in the metal center's oxidation state. Electron donors were also found to have a significant effect on the catalyst activity. Addition of electron donors such as ether-alcohols, ether-esters, amino-alcohols, polymethylhydrosiloxanes, or phosphine oxides to ethylene homopolymerizations resulted in increased activity. When the same electron donors were added to 1-hexene copolymerizations, however, the result was a decrease in the catalytic activity relative to the unperturbed copolymerization.

Based on the above results, Karol and coworkers proposed that competitive equilibria among the aluminum alkyl, electron donor, comonomer, and other ligands for unsaturated transition metal centers might be responsible for the observed effects. The corresponding kinetic model is shown in Figure 2, where [ ] is an unsaturated position, P is an attached live polymer chain, and L represents any coordinating ligand, for example, monomer, Lewis base, or comonomer. The remaining three bonds are assumed to be attached to chlorine atoms or some kind of support.

The above depiction of highly unsaturated vanadium centers includes the notion that the vacant positions may be weakly coordinated with easily removable ligands. From this point of view, active centers are created by the coordination of an activating ligand to an unsaturated metal center, then the remaining vacancy provides a site for monomer coordination prior to chain insertion. Of course, different olefins will create different active sites and will thereby influence the catalytic activity. Thus the description of any given active site should indicate the coordinating ligand at the metal center.

Karol, Kao, and Cann used isomeric dimethoxybenzenes to probe the number of bis-vacant coordination sites present in the $VCl_3(THF)/SiO_2$ system. Using 1,3-dimethoxybenzene at a one-to-one ratio to vanadium, the polymerization activity decreased slightly. The same amount of 1,2-di-

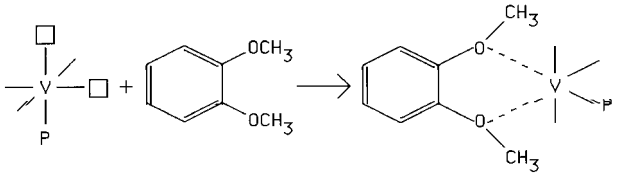

Figure 3 Chelating complex formed between veratrole and an active vanadium center.

methoxybenzene (veratrole), however, resulted in almost total deactivation. This result provides convincing support for a model based on the bis-vacant unsaturated model.

It is believed that the chelating complex shown in Figure 3 is formed between veratrole and the active vanadium center. Thus this irreversible reaction can be used as a probe for titrating active sites. These titration results revealed that only $\sim$ 30% of the vanadium centers were active during ethylene polymerization. Veratrole was also found to be effective in displacing other electron donor ligands, thereby supporting the concept of competitive, dynamic equilibria between the various ligands and the unsaturated transition metal centers.

The idea of competitive ligand coordination at catalyst active centers has also been suggested by other researchers. Kissin,[18] for example, has used such an approach to explain both comonomer and hydrogen rate effects. Using a $TiCl_4/MgCl_2$ catalyst, he performed gas-phase ethylene homopolymerization experiments in the presence and absence of hydrogen in order to study the dependence of polymerization rate on monomer concentration and the kinetic effect of hydrogen.

In studying the effect of monomer concentration, Kissin varied the partial pressure of ethylene over the range 0.28–1.38 MPa. The resulting effect was dramatic and reversible, showing significantly higher polymerization rates at higher partial pressures. Interestingly, when the data were fit using the traditional power expression $R = k_{\text{eff}} P_E^n$, the kinetics were fit best with an order of $n = 1.5$ or 1.6 rather than the usually assumed first-order kinetics. Kissin notes that due to the reversible nature of the phenomenon, an irreversible modification of the active centers is not a valid explanation. The idea that ethylene compressibility could be responsible is also unable to explain the deviation, as it does not change by $> 1\%$. Finally, the effect of total reaction pressure on the order was investigated showing that only the ethylene partial pressure was a factor. Thus Kissin hypothesized that the resulting order might be due to some kind of equilibrium kinetics.

When hydrogen was added to the ethylene polymerizations the rate of polymerization suddenly decreased, but was again restored to its original activity once the hydrogen was used up. Traditionally, it has been proposed that this reduction is due to slow re-initiation of the active center following chain transfer to hydrogen. Kissin points out, however, that the assumption that ethylene insertion into the metal–hydrogen bond is more difficult than insertion into the metal–carbon bond is inconsistent with experimental data from stable ethylene complexes.[19,20] Although hydrogen can theoretically modify the active centers by reducing them to less active oxidation states, the reversibility of the effect again suggests the possibility of some equilibrium process.

Considering the above results, Kissin proposed the following kinetic model. To begin with, the traditional first-order kinetics assume propagation via

$$C^*(E)_x + E \xrightarrow{k_p} C^*(E)_{x+1} \quad R_p = k_p C^* C_m \quad (6)$$

where C^* is the number of active centers and C_m is the monomer concentration. In order to explain reaction orders > 1, Kissin suggests that C^* should also depend on the ethylene concentration in the reactor via the equilibrium reaction

$$C_p^* + E \underset{k_{-1}}{\overset{k_1}{\Leftrightarrow}} C^* \quad K_1 \equiv k_1/k_{-1} = C^*/(C_p^* P_E) \quad (7)$$

where C_p^* is the concentration of potential active centers. Similarly, hydrogen deactivates polymerization centers C^* via the equilibrium reaction

$$C^* + H_2 \underset{k_{-2}}{\overset{k_2}{\Leftrightarrow}} C_{\text{H}}^* \quad K_2 \equiv k_2/k_{-2} = C_{\text{H}}^*/(C^* P_{\text{H}}) \quad (8)$$

where C_H^* is the concentration of deactivated centers. An ethylene/hydrogen site competition reaction such as

$$C^* + \text{H}_2 \underset{k_{-2}}{\overset{k_2}{\Leftrightarrow}} C_{\text{H}}^* + C_2\text{H}_4 \quad (9)$$

cannot be responsible for the deactivation effect as such a model fails to fit the experimental data.

Kissin combined the above equilibrium equations with a balance on the active centers to arrive

at an expression for the polymerization rate as a function of the partial pressures of ethylene (P_E) and hydrogen (P_H):

$$R_p = k_p C_0^* P_E^2/(P_E + K_1^{-1} + K_2 P_E P_H) \quad (10)$$

where C_0^* is the total number of active centers. Defining R_p^0 as the rate in the absence of hydrogen (i.e., when $P_H = 0$), a linear relationship between P_E/R_p^0 and $1/P_E$ was found, thereby lending some credibility to the proposed model. Similarly, a linear correlation between $(1/R_p - 1/R_p^0)$ and P_H/P_E seems to support the postulated equilibrium deactivation by hydrogen.

Kissin also considered other aspects of Ziegler–Natta kinetics in light of the apparently successful equilibrium approach. He notes that ethylene polymerization rates are frequently lower than rates of higher α-olefins despite the much greater intrinsic reactivity of ethylene. In addition, he mentions the rate enhancement effect resulting when comonomers are added to ethylene homopolymerization, when in fact the rates are expected to decrease based on the comonomer reactivity. His explanation for these observations is that each monomer is able to reversibly activate the polymerization centers and that ethylene apparently has a lesser ability to perform this activation.

In modeling the comonomer rate effect, the standard site transformations in Table I can be used to perform reversible ligand coordination reactions to form different types of propagating sites. In cases where such site transformations occur on the same time scale as propagation and/or chain transfer, however, the reactions in Table I yield molecular weights that are unrealistically low. To avoid this problem, it is necessary to permit a no-death site transformation that does not require chain termination with each transformation. This no-death site transformation, included in the general kinetic scheme in Table VII, is also more physically reasonable since the incoming ligand is assumed to coordinate at a vacant position rather than act at the point of chain attachment, as in the case of a true chain transfer reaction.

In addition, as already noted by Kissin, any model must account for propagation orders with respect to monomers that are different from one. Karol and coworkers, for example, found a second-order dependence on ethylene for homopolymerization over titanium and a first-order dependence on ethylene for ethylene-hexene copolymerization over vanadium. While such varying orders may be due to reversible monomer coordination prior to insertion, as suggested by Karol, they might also result from the so-called "trigger" mechanism proposed by Ystenes,[21] whereby propagation requires an incoming monomer M' to trigger insertion of an already complexed monomer M. Although it is possible to write out exact expressions for both reversible monomer coordination and the following auto propagation and/or trigger propagation as done in Table II, it is usually impossible to obtain the required kinetic rate constants. Hence, to account for varying propagation orders with respect to monomer, the propagation rate expression in Table VII has been modified to include this additional parameter.

In concluding this section on modeling the effects of comonomers and other ligands on site kinetics, a few additional remarks regarding the flexibility of the model should be made. For example, although the kinetic scheme in Table I only shows irreversible activation and deactivation, the site transformation reactions may be used to handle reversible activation and deactivation as well. Furthermore, the addition of no-death site transformations allows reversible deactivations without terminating the attached polymer chain. Such no-death transformations may also be used to construct block copolymers or even elastomeric polypropylene having blocks of isotactic and atactic stereosequences, as demonstrated in example 2A. Finally, the site transformation reactions may also be used to simulate a trigger deactivation as shown in Table III, whereby a poison similar in structure to an already coordinated monomer trig-

Table II Monomer Coordination and Propagation Reactions

Reversible or irreversible monomer coordination

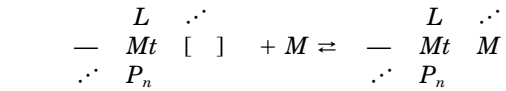

Auto Propagation

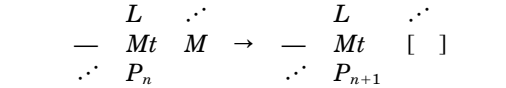

Trigger Propagation

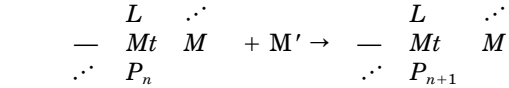

Table III Deactivation Reactions

Reversible or irreversible deactivation by ligand L'

$$\begin{array}{cccccccc} & L & .^{\cdot} & & & & L & .^{\cdot} \\ — & Mt & [\ ] & + L' \rightleftarrows & & — & Mt & L' \\ .^{\cdot} & P & & & & .^{\cdot} & P & \end{array}$$

Trigger deactivation by ligand L'

$$\begin{array}{cccccccc} & L & .^{\cdot} & & & & L & .^{\cdot} \\ — & Mt & M & + L' \rightarrow & & — & Mt & L' \\ .^{\cdot} & P_n & & & & .^{\cdot} & P_{n+1} & \end{array}$$

gers insertion of that monomer while simultaneously deactivating the site.

Long Chain Branching

While recent interest in branching mechanisms has been sparked by the industrial development of newly emerging metallocene catalysts, even traditional vanadium and chromium catalysts have been known to add long chain branches via internal and terminal double bond polymerizations, respectively. As presented in Table I, the standard Ziegler–Natta kinetic scheme does not account for such branching reactions. Thus, in this section we develop the required reactions to form unsaturated dead polymer chains, as well as the reactions for subsequent long chain branch addition.

Beyond having a catalyst that is capable of adding long chain branches, there must be mechanisms for forming unreacted double bonds on dead polymer species. Such unsaturation is typically produced in one of two ways, either by the introduction of a diene species, or by the inherent nature of the chain transfer mechanisms at work in the given system. The basis for modeling the former mechanism is the same as that used to give propylene multiple reactivities for 1,2- and 2,1-insertions. That is, diene monomers are treated as having two different reactive monomer groups (M_i) and the diene monomer balance is adjusted accordingly. Polymer formed with such dienes will then have unreacted double bonds hanging off the chain, which can eventually react at an active site to form a tetra-functional branch point via the internal double bond branching reaction. The unsaturation which results from the latter chain transfer mechanism can react similarly to create a tri-functional branch point via the terminal double bond branching reaction.

Resconi et al.[22] have investigated the chain transfer mechanisms which lead to terminal unsaturation and have found that the specific mechanisms at work depend greatly on the given catalyst and specific reaction conditions. As shown in Table IV, the primary chain transfer mechanisms at work in the polymerization of propylene are β-hydrogen and β-methyl elimination, as well as small amounts of chain transfer to aluminum cocatalyst.

Chain transfer to the aluminum cocatalyst produces saturated end groups and can thus already be modeled using the standard chain transfer reactions presented in Table I. In systems where β-hydrogen elimination is the only chain transfer mechanism, the observed unsaturated propyl and isopropenyl end groups are believed to be produced by mechanism A in Table V. In systems where β-methyl elimination occurs, one observes unsaturated isopropyl end groups thought to be formed via reaction B, as well as allylic end groups most likely produced as shown in reactions C and D. The preference for β-methyl versus β-hydrogen elimination using certain catalyst systems has been attributed to lower steric hindrance in the transition state of the former reaction.

Another source of unsaturation is the result of chain transfer to monomer, as suggested in a number of papers. Tsutsui, Kashiwa, and Mizuno,[12] for example, have obtained saturated propyl and unsaturated isopropenyl groups when polymerizing propylene in the absence of hydrogen. They attribute the formation of these end groups to chain transfer with monomer, as shown in reaction E of Table VI. In another paper, Chien and He[23] have suggested σ-bond metathesis, reaction F, which produces dead polymer and a terminal double bond at the catalyst active site.

Since both chain transfer to monomer and σ-bond metathesis each result in the production of one terminal double bond (TDB), the model in Table I needs an additional monomer chain transfer reaction that forms dead polymer having an unsaturated terminal double bond end group ($e = utdb$). Similarly, the β-hydrogen and β-methyl elimination reactions can be modeled using a spontaneous chain transfer reaction to form dead polymer having the terminal double bond end group. These additions to the standard kinetic scheme are presented in the more general kinetic scheme in Table VII.

The branching reactions themselves can be thought of much like the basic propagation reaction. In the case of terminal double bond polymer-

Table IV Percentages of Chain Transfer Mechanisms at Work in the Polymerization of Propylene as Calculated from Relative Intensities of Different End Groups

Metallocene	T_p (°C)	β-H	β-Me	Al-transfer
$C_{p2}ZrCl_2$	50	100	—	—
$C_{p2}ZrCl_2$	0	100	—	—
$C_{p2}HfCl_2$	50	100	—	—
$^*C_{p2}ZrCl_2$	50	7.9	91.1	—
$^*C_{p2}ZrCl_2$	0	7.1	81.8	1
$^*C_{p2}ZrCl_2$	−40	—	—	11.1
$^*C_{p2}HfCl_2$	50	2	98	traces
$^*C_{p2}HfCl_2$	0	2.0	62.7	35.3

(C_p = cyclopentadienyl and $^*C_p$ = pentamethylcyclopentadienyl)[22]

ization the analogy with the standard propagation is obvious; the unsaturated end of the dead polymer acts like the double bond of an α-olefin monomer having a very long tail. This reaction may be represented as shown in eqs. (11) and (12), where an additional index (b) is required to count the number of branches formed by TDB-insertion.

$$P^k_{\underline{n},b,j} + D^l_{\underline{m},t,i=utdb} \rightarrow P^k_{\underline{n}+\underline{m},b+t+1,e=rtdb} \quad (11)$$

$$R^k_{TDBij} = k^k_{TDBij} P^k_{\underline{n},b,j} (D^l_{\underline{m},t,i=utdb})_{\text{eff}}. \quad (12)$$

Following branch addition the polymer end group changes to reacted terminal double bond ($rtdb$) in recognition of the fact that further propagation at this tri-functional branch point will be sterically hindered. Furthermore, just as with other bulk species, an effectiveness factor can be specified to account for the fact that the concentration of dead polymer at the active site may be different from that of the bulk phase.

Internal double bond polymerization takes place by means of a similar reaction between live polymer chains and the free internal double bonds located along the dead polymer chains. Han-Adebekun[24] has suggested the representation shown in eq. (13) where yet another index ($\underline{d}$) is added to count the number of free internal double bonds of each type.

$$P^k_{\underline{n},\underline{d},b,i} + D^l_{\underline{m},\underline{c},t,z} \rightarrow P^k_{\underline{n}+\underline{m},\underline{d}+\underline{c}-\delta_j,b+t,j} \quad (13)$$

As shown in eq. (13) a free idb of type j reacts at an occupied site to produce a tetrafunctional branched polymer having the end group of the

Table V Spontaneous Unsaturation Reactions[22]

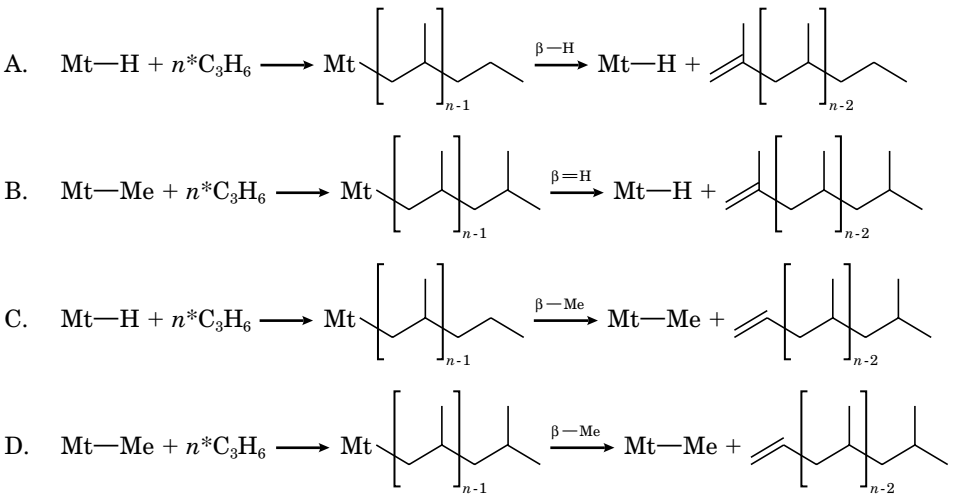

Table VI Monomer Induced Unsaturation Reactions

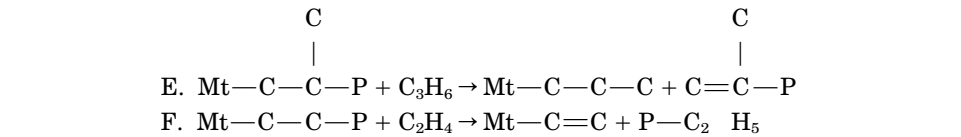

reacting free *idb* type j. In such a scheme the number of branches would then have to be calculated via the difference between the number of reacted dienes in $\underline{n}$ and the number of free internal double bonds in $\underline{d}$.

To be consistent with the TDB branching reaction and for simplicity to be gained later when deriving moment equations, the IDB branching reaction in eq. (13) can be modified as shown in eq. (14).

$$P^k_{\underline{n},\underline{d},b,i} + D^l_{\underline{m},\underline{c},t,z} \rightarrow P^k_{\underline{n}+\underline{m},\underline{d}+\underline{c}+\underline{\delta}_j,b+t,e=ridb}. \quad (14)$$

Here the index $\underline{d}$ is now used to count the number of branches formed by each type of IDB, and the resulting end group is the reacted internal double bond (*ridb*) type, which again accounts for the fact that propagation following branch addition will certainly have a different reactivity due to steric hindrance.

In developing the rate expression for reaction (14), one must account for the fact that the reactivity of the dead species will depend on the number of free internal double bonds present. To demonstrate how this is done, start by considering the dead polymer species $D^k_{\underline{m},\underline{c},t,z}$ to be reacted. The first column vector index $\underline{m}$ gives the number of each monomer group reacted to form the molecule ($\underline{m}^T = [m_1, m_2, m_3 = \text{idb}_1, m_4 = \text{idb}_2]$). As shown, the maximum number of monomers (*nmon*) is three and the maximum number of monomer groups is *nmon* + 1 = 4 due to the presence of the diene. Here m_1 and m_2 have single reactivities, while the third diene monomer has two reactive

Table VII A General Kinetic Scheme for Catalyzed Olefin Polymerization

Activation	$C_{pot} + A \rightarrow P^k_o$	$R^k_{aA} = k^k_{\text{aA}} C_{pot} C^{O^k_{aA}}_{A,eff}$
	$C_{pot} \rightarrow P^k_o$	$R^k_{aSp} = k^k_{aSp} C^{O^k_{aSp}}_{pot}$
Initiation	$P^k_o + M_i \rightarrow P^k_{\underline{\delta}_i,i}$	$R^k_{pi} = k^k_{pi} P^k_o C_{M_i,eff}$
Propagation	$P^k_{\underline{n},\underline{d},b,j} + M_i \rightarrow P^k_{\underline{n}+\underline{\delta}_i,\underline{d},b,i}$	$R^k_{pij} = k^k_{pij} P^k_{\underline{n},\underline{d},b,j} C^{O^k_{pij}}_{M_i,eff}$
Chain Transfer	$P^k_{\underline{n},\underline{d},b,j} + T \rightarrow P^l_o + D^k_{\underline{n},\underline{d},b,j}$	$R^{kl}_{cTj} = k^{kl}_{cTj} P^k_{\underline{n},\underline{d},b,j} C^{O^{kl}_{cTj}}_{T,eff}$
	$P^k_{\underline{n},\underline{d},b,j} + M_i \rightarrow P^l_{\underline{\delta}_i,i} + D^k_{\underline{n},\underline{d},b,j}$	$R^{kl}_{cM_ij} = k^{kl}_{cM_ij} P^k_{\underline{n},\underline{d},b,j} C^{O^{kl}_{cM_ij}}_{M_i,eff}$
	$P^k_{\underline{n},\underline{d},b,j} \rightarrow P^l_o + D^k_{\underline{n},\underline{d},b,j}$	$R^{kl}_{cSpj} = k^{kl}_{\text{cSpj}} P^k_{\underline{n},\underline{d},b,j}$
Unsaturation	$P^k_{\underline{n},\underline{d},b,j} \rightarrow P^l_o + D^k_{\underline{n},\underline{d},b,e}$	$R^{kl}_{uSpj} = k^{kl}_{\text{uSpj}} P^k_{\underline{n},\underline{d},b,j}$
	$P^k_{\underline{n},\underline{d},b,j} + M_i \rightarrow P^l_{\underline{\delta}_i,i} + D^k_{\underline{n},\underline{d},b,e}$	$R^{kl}_{uM_ij} = k^{kl}_{uM_ij} P^k_{\underline{n},\underline{d},b,j} C^{O^{kl}_{uM_ij}}_{M_i,eff}$
Transformation	$P^k_o + X \rightarrow P^l_o$	
(death or no-death)	$P^k_{\underline{n},\underline{d},b,j} + X \rightarrow P^l_o + D^k_{\underline{n},\underline{d},b,j}$ or $P^l_{\underline{n},\underline{d},b,j}$	$R^{kl}_{tL} = k^{kl}_{tL}(P^k_o + P^k_{\underline{n},\underline{d},b,j}) C^{O^{kl}_{tL}}_{X,eff}$
	$P^k_o \rightarrow P^l_o$	$R^{kl}_{tSp} = k^{kl}_{tSp}(P^k_o + P^k_{\underline{n},\underline{d},b,j})$
	$P^k_{\underline{n},\underline{d},b,j} \rightarrow P^l_o + D^k_{\underline{n},\underline{d},b,j}$ or $P^l_{\underline{n},\underline{d},b,j}$	
Deactivation	$P^k_o + X \rightarrow C_d$	$R^k_{dX} = k^k_{dX}(P^k_o + P^k_{\underline{n},\underline{d},b,j}) C^{O^k_{dX}}_{X,eff}$
	$P^k_{\underline{n},\underline{d},b,j} + X \rightarrow C_d + D^k_{\underline{n},\underline{d},b,j}$	
	$P^k_o \rightarrow C_d$	$R^k_{dSp} = k^k_{dSp}(P^k_o + P^k_{\underline{n},\underline{d},b,j})$
	$P^k_{\underline{n},\underline{d},b,j} \rightarrow C_d + D^k_{\underline{n},\underline{d},b,j}$	
Branching	$P^k_{\underline{n},\underline{d},b,j} + D^l_{\underline{m},\underline{c},t,i=utdb} \rightarrow P^k_{\underline{n}+\underline{m},\underline{d}+\underline{c},b+t+1,e=rtdb}$	
	$R^k_{TDBij} = k^k_{\text{TDBij}} P^k_{\underline{n},\underline{d},b,j} (D^l_{\underline{m},\underline{c},t,i=utdb})_{eff}$	
	$P^k_{\underline{n},\underline{d},b,i} + D^l_{\underline{m},\underline{c},t,z} \rightarrow P^k_{\underline{n}+\underline{m},\underline{d}+\underline{c}+\underline{\delta}_j,b+t,e=ridb}$	
	$R^k_{IDBji} = k^k_{IDBji} P^k_{\underline{n},\underline{d},b,i} (D^l_{\underline{m},\underline{c},t,z})_{eff} [\underline{\delta}_{nmon+j-1} \times \underline{m} - \underline{\delta}_j \times \underline{c}]$	

double bonds, as represented by monomer groups m_3 and m_4. The second column vector index $\underline{c}$ counts the number of branches formed by reaction of free internal double bonds of type 2 and type 1, respectively ($\underline{c}^T = [c_1 = \text{idb}_2, c_2 = \text{idb}_1]$). Then, using a Kronecker delta of dimension two, one can obtain the total number of free internal double bonds from the relation given in eq. (15) where j indexes the type of free internal double bond reacting.

$$[\underline{\delta}_{nmon+j-1} \times \underline{m} - \underline{\delta}_j + \underline{c}] \qquad (15)$$

Thus $j = 1$ refers to the situation where a free IDB of type 2 reacts to form a branch (idb_2) and $j = 2$ refers to the case where a free IDB of type 1 reacts to form a branch (idb_1). The resulting rate expression for the IDB branching reaction in eq. (14) is given in eq. (16).

$$R^k_{\text{IDB}ji} = k^k_{\text{IDB}ji} P^k_{\underline{n},\underline{d},b,i} (D^l_{\underline{m},\underline{c},t,z})_{\text{eff}} [\underline{\delta}_{nmon+j-1} \times \underline{\text{m}} - \underline{\delta}_j \times \underline{c}]. \qquad (16)$$

GENERALIZED KINETIC MODELING

Having developed the general kinetic scheme in Table VII, it is now possible to apply the method of moments to these reactions in order to obtain a system of differential equations which may be numerically integrated. Although the kinetic nomenclature has already been defined on an as-needed basis, the definitions are provided in summary form in Table VIII. As shown, each polymer chain is characterized by the site type at which it is growing, its incorporated monomers, the number of tetra-functional branches formed via the IDB mechanism, the number of tri-functional branches formed via the TDB mechanism, and the end group type. While the general kinetic scheme is not restricted to any specific number of site types, monomers, etc., the dimensions shown in Table VIII are those implemented in the POLYRED™ simulation package[2] and used to create the examples for this paper.

Before applying the method of moments to the kinetic scheme in Table VII, it is necessary to adopt the operational definitions originally suggested by Arriola[25] and provided in Table IX. These mathematical relationships are required for both defining the live and bulk polymer moments given in Table X, and for providing a means of transforming the individual kinetic reactions into moment balance equations.

Table VIII Kinetic Nomenclature Summary

Potential Site:	C_{pot}	Dead Site:	C_d
Vacant Site:	P^k_o	Live Polymer:	$P^k_{\underline{n},\underline{d},b,j}$
Initiated Site:	$P^k_{\underline{\delta}_j,i}$	Dead Polymer:	$D^k_{\underline{n},\underline{d},b,j}$
Site Type:	k = 1, 2, 3, or 4		
Monomers:	$\underline{n} = [m_1, m_2, m_3 = idb_1, m_4 = idb_2]$		
IDB Branches:	$\underline{d} = [idb_2, idb_1]$		
TDB Branches:	$b = [tdb]$		
End Group Type:	$j = m_1, m_2, m_3, m_4, ridb, rtdb, utdb$		

To develop the general differential moment balance equations, live and dead polymer chain balances must be applied to each reaction of the kinetic scheme. Using the initiation reaction as an example, the live polymer chain balance yields the individual production term given in eq. (17).

$$\frac{dP^k_{\underline{\delta}j,\underline{0},0,j}}{dt} = k^k_{pj} P^k_0 C_{Mj,\text{eff}}. \qquad (17)$$

Application of the definition of the live polymer moment to this polymer chain balance then yields the result shown in eq. (18).

$$\frac{d\mu^k_{\underline{f},\underline{h},r,j}}{dt} = \frac{d}{dt}\left[\sum_{\underline{\delta}_j}^{\underline{\delta}_j} \sum_{\underline{d}=\underline{0}}^{\underline{0}} \sum_{b=0}^{0} \underline{\delta}^f_j \underline{d}^h b^r k^k_{pj} P^k_0 C_{Mj,\text{eff}}\right]$$
$$= \underline{\delta}^f_j \underline{0}^h 0^r k^k_{pj} P^k_0 C_{Mj,\text{eff}}. \qquad (18)$$

Continuing in this fashion with the remaining kinetic equations produces the set of general differential moment balance equations summarized in Tables XI and XII.

With regard to the summation limits in Tables XI and XII it should be mentioned that *nsite* is the number of site types, *nmong* is the number of monomer groups, *negl* is the number of end group types allowed on the live polymer, *neg* is the number of end group types allowed on the bulk polymer, and *nidb* is the number of internal double bond types. Also notice the use of the Kronecker delta in the branching reactions to indicate that a particular term of the moment equation exists only when considering a specific end group type.

Table IX Vector Operations

Kronecker Delta: $\delta(i-j) \equiv \begin{cases} 0 & \text{if } i \neq j \\ 1 & \text{if } i = j \end{cases}$

Unit Vector: $\underline{\delta}_j \equiv [0, 0, \cdots \delta_j = 1, \cdots 0, 0]$

Vector Exponentiation: $\underline{n}^{\underline{f}} \equiv \prod_{i=1}^{m} (n_i)^{f_i}$

Vector Summation: $\sum_{\underline{n}=\underline{0}}^{\underline{f}} \equiv \prod_{i=1}^{m} \left(\sum_{n_i=0}^{f_i} \right)$

Vector Binomial: $\binom{\underline{f}}{\underline{n}} \equiv \prod_{i=1}^{m} \binom{f_i}{n_i}$ where $\binom{f}{n} \equiv \frac{f!}{n!(f-n)!}$

Starting from the general moment expressions it is then possible to generate the specific moment equations[26] required for both moment closure and the particular polymer properties of interest. When considering nonbranched systems, the set of moments given in the second column of Table XIII satisfies the above requirements. As demonstrated in Table XIV, this small set of moments is sufficient for calculating number (D_n^k) and weight (D_w) average chain lengths, polymer composition (F_{pi}^k), fractions of each end group type on the polymer chains (BFEG_j^k), as well as several other useful properties.[1] When modeling branched systems, however, it is necessary to use the set of moments given in the third column of Table XIII. The most obvious difference is the significant increase in the number of moments required for describing the branching characteristics of the polymer. As shown in Table XV, randomly branched polymers not only have molecular weight distributions, but also branch-point distributions. Here the number average degree of branching (B_n) is obtained by dividing the total number of branches of each type (idb_1, idb_2, or tdb) by the total number of chains, and the weight average degree of branching (B_w) is obtained by ratioing the number of branches of each type weighted by the size of the chain to the number of branches of each type. A more subtle difference is the loss of site specific information on bulk polymer chains required for moment closure. Although this necessarily means that it is no longer possible to consider how bulk polymer properties differ from site to site, it is reasonable considering the fact that individual polymer molecules may contain branches made at different site types anyway. Furthermore, using such a moment structure allows no-death site transformations, which can generate polymer chains that have been constructed under the influence of several different site environments.

Table X Moment Definitions

Live Moments: $\mu_{\underline{f},\underline{h},r,j}^k \equiv \sum_{\underline{n}=\underline{0}}^{\infty} \sum_{\underline{d}=\underline{0}}^{\infty} \sum_{\underline{b}=0}^{\infty} \underline{n}^{\underline{f}} \underline{d}^{\underline{h}} b^r P_{\underline{n},\underline{d},b,j}^k$

Bulk Moments: $\lambda_{\underline{f},\underline{h},r,j}^k \equiv \sum_{\underline{n}=\underline{0}}^{\infty} \sum_{\underline{d}=\underline{0}}^{\infty} \sum_{\underline{b}=0}^{\infty} \underline{n}^{\underline{f}} \underline{d}^{\underline{h}} b^r (P_{\underline{n},\underline{d},b,j}^k + D_{\underline{n},\underline{d},b,j}^k$

EXAMPLES

In this section some of the features and capabilities of the general kinetic model are demonstrated by attempting to duplicate experimental observations available in the published Ziegler–Natta literature. Many researchers have spent lifetimes investigating the effects discussed here, and this work in no way claims to resolve them. Rather, the intent of the examples given here is to simply demonstrate how the model may be applied to obtain a better understanding of the underlying fundamentals.

Hydrogen Rate Effects

As discussed previously, the effect of hydrogen on a particular polymerization can vary greatly depending on the reaction conditions and the specific choice of catalyst. In example 1A we consider

Table XI Live Moments of the General Kinetic Scheme

Live Moments	$R\mu^{k}_{\underline{f},\underline{h},r,j} =$
Initiation	$+ \underline{0}^{h}0^{r}\delta^{f}_{f}k^{k}_{pj}P^{k}_{o}C_{M_j,eff}$
Propagation	$+ \sum_{i}^{negl} k^{k}_{pji}C^{O^{k}_{pji}}_{M_j,eff} \sum_{\underline{g}=0}^{\underline{f}} \binom{f}{g} \underline{\delta}^{f-g}_{j}\mu^{k}_{\underline{g},\underline{h},r,i} - \sum_{i}^{nmong} k^{k}_{pij}C^{O^{k}_{pij}}_{M_i,eff}\mu^{k}_{\underline{f},\underline{h},r,j}$
Chain Transfer	$+ \sum_{l=1}^{nsite}\left[\underline{0}^{h}0^{r}\delta^{f}_{f}\sum_{i=1}^{negl} k^{lk}_{cMji}C^{O^{lk}_{cMji}}_{M_j,eff}\mu^{l}_{\underline{0},\underline{0},0,i} - \sum_{i=1}^{nmong} k^{kl}_{cMij}C^{O^{kl}_{cMij}}_{M_i,eff}\mu^{k}_{\underline{f},\underline{h},r,j}\right]$
	$- \sum_{l=1}^{nsite}\left[k^{kl}_{cHj}C^{O^{kl}_{cHj}}_{H,eff} + k^{kl}_{cAj}C^{O^{kl}_{cAj}}_{A,eff} + k^{kl}_{cEj}C^{O^{kl}_{cEj}}_{E,eff} + k^{kl}_{cSj}C^{O^{kl}_{cSj}}_{S,eff} + k^{kl}_{cTj}C^{O^{kl}_{cTj}}_{T,eff} + k^{kl}_{cSpj}\right]\mu^{k}_{\underline{f},\underline{h},r,j}$
TDB Unsaturation Spontaneous	$- \sum_{l=1}^{nsite} k^{kl}_{uSpj}\mu^{k}_{\underline{f},\underline{h},r,j}$
TDB Unsaturation by Monomer	$+ \sum_{l=1}^{nsite}\left[\underline{0}^{h}0^{r}\delta^{f}_{f}\sum_{i=1}^{negl} k^{lk}_{uMji}C^{O^{lk}_{uMji}}_{M_j,eff}\mu^{l}_{\underline{0},\underline{0},0,i} - \sum_{i=1}^{nmong} k^{kl}_{uMij}C^{O^{kl}_{uMij}}_{M_i,eff}\mu^{k}_{\underline{f},\underline{h},r,j}\right]$
Death Site Transformation	$- \sum_{l=1}^{nsite}\left[\sum_{i=1}^{nmong} k^{kl}_{tMi}C^{O^{kl}_{tMi}}_{M_i,eff} + \alpha^{kl}\right]\mu^{k}_{\underline{f},\underline{h},r,j}$
No-Death Site Transformation	$+ \sum_{l=1}^{nsite}\left[\sum_{i=1}^{nmong} k^{lk}_{tMi}C^{O^{lk}_{tMi}}_{M_i,eff} + \alpha^{lk}\right]\mu^{l}_{\underline{f},\underline{h},r,j} - \sum_{l=1}^{nsite}\left[\sum_{i=1}^{nmong} k^{kl}_{tMi}C^{O^{kl}_{tMi}}_{M_i,eff} + \alpha^{kl}\right]\mu^{k}_{\underline{f},\underline{h},r,j}$
TDB Branching	$+ \delta(j - rtdb)\sum_{i=1}^{negl}\sum_{e=utdb} k^{k}_{TDBei}\sum_{\underline{g}=0}^{\underline{f}}\binom{f}{g}\sum_{\underline{s}=0}^{\underline{h}}\binom{h}{s}\sum_{a=0}^{r}\binom{r}{a}\sum_{w=0}^{a}\binom{a}{w}\mu^{k}_{\underline{f}-\underline{g},\underline{h}-\underline{s},r-a,i}\lambda_{\underline{g},\underline{s},w,e}$
	$- \sum_{e=utdb} k^{k}_{TDBej}\lambda_{\underline{0},\underline{0},0,e}\mu^{k}_{\underline{f},\underline{h},r,j}$
IDB Branching	$- \sum_{i=1}^{nidb} k^{k}_{IDBij}\mu^{k}_{\underline{f},\underline{h},r,j}[\lambda_{\underline{\delta}_{nmon+i-1},\underline{0},0} - \lambda_{\underline{0},\underline{\delta}_{i},0}] + \delta(j - ridb)\sum_{i=1}^{negl}\sum_{e=1}^{nidb} k^{k}_{IDBei}$
	$\times \sum_{\underline{g}}^{\underline{f}}\binom{f}{g}\sum_{\underline{s}}^{\underline{h}}\binom{h}{s}\sum_{\underline{w}}^{\underline{s}}\binom{s}{w}\sum_{a}^{r}\binom{r}{a}\underline{\delta}^{s-w}_{e}\mu^{k}_{\underline{f}-\underline{g},\underline{h}-\underline{s},r-a,i}[\lambda_{\underline{g}+\underline{\delta}_{nmon+e-1},\underline{w},a} - \lambda_{\underline{g},\underline{w}+\underline{\delta}_{e},a}]$
Irreversible Deactivation	$- \left[\sum_{i=1}^{negl} k^{k}_{dMi}C^{O^{k}_{dMi}}_{M_{ii},eff} + k^{k}_{dH}C^{O^{k}_{dH}}_{H,eff} + k^{k}_{dA}C^{O^{k}_{dA}}_{A,eff} + k^{k}_{dB}C^{O^{k}_{dB}}_{B,eff} + k^{k}_{dE}C^{O^{k}_{dE}}_{E,eff} + k^{k}_{dX}C^{O^{k}_{dX}}_{X,eff} + k^{k}_{dSp}\right]\mu^{k}_{\underline{f},\underline{h},r,j}$
where	$\alpha^{kl} \equiv k^{kl}_{tH}C^{O^{kl}_{tH}}_{H,eff} + k^{kl}_{tA}C^{O^{kl}_{tA}}_{A,eff} + k^{kl}_{tE}C^{O^{kl}_{tE}}_{E,eff} + k^{kl}_{tS}C^{O^{kl}_{tS}}_{S,eff} + k^{kl}_{tX}C^{O^{kl}_{tX}}_{X,eff} + k^{kl}_{tSp}$

the rate reduction of ethylene polymerization due to a proposed deactivation of the catalyst sites by hydrogen. Then, in examples 1B and 1C, an attempt is made to explain propylene polymerization rate enhancement on the basis of hydrogen "cleaning" of the pseudo-dormant sites which remain following reverse 2,1-insertion. Although the simple models considered here each address only one possible explanation for the hydrogen effect, it should be remembered that there may actually be several causes that are acting simultaneously to produce the observed net rate effect.

Example 1A: Rate Reduction in Ethylene Polymerization

In this example we use the simple model shown in Figure 4 to simulate the rate reduction obtained experimentally by Kim, Kim, and Woo[27] upon introducing hydrogen into ethylene polymerization over a highly active silica-supported $TiCl_4/MgCl_2$ catalyst. Both the original experiments and the simulations performed here were in a 1-L batch reactor at 80°C with ethylene feed to maintain constant pressure.

According to the simple model in Figure 4, the alkyl cocatalyst (triethylaluminum) creates an active site P^1_0 which is then modified by ethylene to form a propagating site P^2_0. The polymer molecular weight is then controlled by chain transfer to monomer and chain transfer to hydrogen when present. As demonstrated in Figure 5, the presence of hydrogen does not appear to affect the catalyst decay profile; rather, hydrogen seems to reduce the reactivity of the catalyst by simply re-

Table XII Bulk Moments of the General Kinetic Scheme

Bulk Moments	$R_{\lambda^{k}_{\underline{f},\underline{h},r,j}} =$
Initiation	$+ \underline{0^h}0^r\delta^f_j k^k_{pj} P^k_o C_{M_j,eff}$
Propagation	$+ \sum_{i}^{negl} k^k_{pji} C^{O^k_{pji}}_{M_j,eff} \sum_{\underline{g}=0}^{\underline{f}} \binom{f}{\underline{g}} \underline{\delta^{f-g}_j} \mu^k_{\underline{g},\underline{h},r,i} - \sum_{i}^{nmong} k^k_{pij} C^{O^k_{pij}}_{M_i,eff} \mu^k_{\underline{f},\underline{h},r,j}$
Chain Transfer	$+ \sum_{l=1}^{nsite} \underline{0^h}0^r\underline{\delta^f_j} \sum_{i=1}^{negl} k^{lk}_{cMji} C^{O^{lk}_{cMji}}_{M_j} \mu^l_{\underline{0},\underline{0},\underline{0},i}$
TDB Unsaturation Spontaneous	$+ \sum_{l=1}^{\text{nsite}} \left[\delta(j - utdb) \sum_{i=1}^{negl} k^{kl}_{uSpi} \mu^k_{\underline{f},\underline{h},r,i} - k^{kl}_{uSpj} \mu^k_{\underline{f},\underline{h},r,j} \right]$
TDB Unsaturation by Monomer	$+ \sum_{l=1}^{nsite} \left[\underline{0^h}0^r\underline{\delta^f_j} \sum_{i=1}^{negl} k^{lk}_{uMji} C^{O^{lk}_{uMji}}_{M_j,eff} \mu^l_{\underline{0},\underline{0},\underline{0},i} \right.$
	$\left. - \sum_{i=1}^{nmong} \left(k^{kl}_{uMij} C^{O^{kl}_{uMij}}_{M_i,eff} \mu^k_{\underline{f},\underline{h},r,j} - \delta(j - utdb) \sum_{e=1}^{Nmgr} k^{kl}_{uMie} C^{O^{kl}_{uMie}}_{M_i,eff} \mu^k_{\underline{f},\underline{h},r,e} \right) \right]$
Death Site Transformation	$+ 0$
No-Death Site Transformation	$+ \sum_{l=1}^{nsite} \left[\sum_{i=1}^{nmong} k^{lk}_{tMi} C^{O^{lk}_{tMi}}_{M_i,eff} + \alpha^{lk} \right] \mu^l_{\underline{f},\underline{h},r,j} - \sum_{l=1}^{nsite} \left[\sum_{i=1}^{nmong} k^{kl}_{tMi} C^{O^{kl}_{tMi}}_{M_i,eff} + \alpha^{kl} \right] \mu^k_{\underline{f},\underline{h},r,j}$
TDB Branching	$+ \delta(j - rtdb) \sum_{i=1}^{negl} \sum_{e=utdb} k^k_{TDBei} \sum_{\underline{g}=0}^{\underline{f}} \binom{f}{\underline{g}} \sum_{\underline{s}=0}^{\underline{h}} \binom{h}{\underline{s}} \sum_{a=0}^{r} \binom{r}{a} \sum_{w=0}^{a} \binom{a}{w} \mu^k_{\underline{f}-\underline{g},\underline{h}-\underline{s},r-a,i} \quad \lambda_{\underline{g},\underline{s},w,e}$
	$- \sum_{e=utdb} k^k_{TDBej} \lambda_{\underline{0},\underline{0},\underline{0},e} \mu^k_{\underline{f},\underline{h},r,j} - \delta(j - utdb) \sum_{i=1}^{negl} \sum_{l=1}^{nsite} k^l_{TDBji} \mu^l_{\underline{0},\underline{0},\underline{0},i} \lambda^k_{\underline{f},\underline{h},r,j}$
IDB Branching	$- \sum_{i=1}^{nidb} k^k_{IDBij} \mu^k_{\underline{f},\underline{h},r,j} \left[\lambda_{\underline{\delta}_{nmom+i-1},\underline{0},0} - \lambda_{\underline{0},\underline{\delta}_i,0} \right] + \delta(j - ridb) \sum_{i=1}^{negl} \sum_{e=1}^{nidb} k^k_{IDBei}$
	$\times \sum_{\underline{g}}^{\underline{f}} \binom{f}{\underline{g}} \sum_{\underline{s}}^{\underline{h}} \binom{h}{\underline{s}} \sum_{\underline{w}}^{\underline{s}} \binom{s}{\underline{w}} \sum_{a}^{r} \binom{r}{a} \underline{\delta^{s-w}_e} \mu^k_{\underline{f}-\underline{g},\underline{h}-\underline{s},r-a,i} \left[\lambda_{\underline{g}+\underline{\delta}_{nmom+e-1},\underline{w},a} - \lambda_{\underline{g},w+\underline{\delta}_e,a} \right]$
	$- \sum_{i=1}^{nibd} \sum_{z=1}^{negl} \sum_{l=1}^{nsite} k^l_{lDBiz} \mu^l_{\underline{0},\underline{0},\underline{0},z} \left[\lambda^k_{\underline{f}+\underline{\delta}_{nmom+i-1},\underline{h},r,j} - \lambda^k_{\underline{f},\underline{h}+\underline{\delta}_i,r,j} \right]$
Irreversible Deactivation	$+ 0$

Table XIII Moment Structures Required for Polymer Properties and Closure

Moment	Non-Branched	Branched
Live Zeroth	$\mu^k_{\underline{0},j}$	$\mu^k_{\underline{0},\underline{0},\underline{0},j}$
Live First	$\mu^k_{\underline{\delta}_m}$	$\mu^k_{\underline{\delta}_m,\underline{0},0}$ $\mu^k_{\underline{0},\underline{\delta}_m,0}$ $\mu^k_{\underline{0},\underline{0},1}$
Bulk Zeroth	$\lambda^k_{\underline{0},j}$	$\lambda_{\underline{0},\underline{0},\underline{0},0}$ $\lambda_{\underline{0},\underline{0},\underline{0},j=utdb}$
Bulk First	$\lambda^k_{\underline{\delta}_m}$	$\lambda_{\underline{\delta}_m,\underline{0},0}$ $\lambda_{\underline{0},\underline{\delta}_m,0}$ $\lambda_{\underline{0},\underline{0},1}$
Bulk Second	λ_2	$\lambda_{\underline{\delta}_m+\underline{\delta}_n,\underline{0},0}$ $\lambda_{\underline{0},\underline{\delta}_m+\underline{\delta}_n,0}$ $\lambda_{\underline{\delta}_m,\underline{\delta}_n,0}$ $\lambda_{\underline{\delta}_m,\underline{0},1}$

Table XIV Some Bulk Polymer Properties in Each Moment Structure

Non-Branched	Branched
$DP_n^k = \frac{\lambda_1^k}{\lambda_0^k} = \frac{\sum_{m=1}^{nmong} \lambda_{\underline{\delta}_m}^k}{\sum_{j=1}^{neg} \lambda_{\underline{0},j}^k}$	$DP_n = \frac{\lambda_{1,0,0}}{\lambda_{0,0,0}} = \frac{\sum_{i=1}^{nmong} \lambda_{\underline{\delta}_i,\underline{0},0}}{\lambda_{\underline{0},\underline{0},0}}$
$DP_w = \frac{\lambda_2}{\lambda_1} = \frac{\lambda_2}{\sum_{k=1}^{nsite} \sum_{m=1}^{nmong} \lambda_{\underline{\delta}_m}^k}$	$DP_w = \frac{\lambda_{2,0,0}}{\lambda_{1,0,0}} = \frac{\sum_{m=1}^{nmong} \sum_{n=1}^{nmong} \sum_{j=1}^{neg} \lambda_{\underline{\delta}_m + \underline{\delta}_n, 0, 0, j}}{\sum_{m=1}^{nmong} \sum_{j=1}^{neg} \lambda_{\underline{\delta}_m,\underline{0},0,j}}$
$F_{pi}^k = \frac{\lambda_{\underline{\delta}_m}^k}{\lambda_1^k} = \frac{\lambda_{\underline{\delta}_m}^k}{\sum_{m=1}^{nmong} \lambda_{\underline{\delta}_m}^k}$	$F_{pi} = \frac{\lambda_{\underline{\delta}_m,0,0}}{\lambda_{1,0,0}} = \frac{\lambda_{\underline{\delta}_m,\underline{0},0}}{\sum_{m=1}^{nmong} \lambda_{\underline{\delta}_m,\underline{0},0}}$
$BFEG_j^k = \frac{\lambda_{\underline{0},j}^k}{\lambda_0^k} = \frac{\lambda_{\underline{0},j}^k}{\sum_{j=1}^{neg} \lambda_{\underline{0},j}^k}$	$Futdb = \frac{\lambda_{\underline{0},\underline{0},0,j=utdb}}{\lambda_{\underline{0},\underline{0},0}}$

ducing the number of sites available for polymerization. Hence the model in Figure 4 includes hyhydrogen deactivation of the potential sites by simply using an activation reaction to create a nonpropagating site P_0^3.

Although the experiments of Kim, Kim, and Woo[27] were performed in slurry, the reaction conditions were adjusted so that both internal and external mass transfer resistance were absent. Assuming polymer at the catalyst surface is 100% amorphous,[28] this absence of diffusion limitations allows one to further assume that the species concentrations at the active sites are equal to those sorbed in 100% amorphous polymer. Thus, here we allow the concentration differences between the bulk phase and catalyst surface to be accounted for and represented by a lumped rate constant as reported by Kim, Kim, and Woo.

The actual parameters used by the model with 1.4 kg/cm^2 hydrogen are given in Table XVI. The number of active sites and the corresponding propagation rate constant are based on the value determined by Kim, Kim, and Woo using the carbon monoxide inhibition method. The number average molecular weight data in Table XVII were used to establish the values of the chain transfer constants for both chain transfer to ethylene and hydrogen. In the case of hydrogen, the data were best fit using a 0.5 order dependence on concentration. Although it is often suggested that hydrogen and ethylene can affect the sites reversibly, the current simulation conditions did not require this feature. Thus, the forward rates specified in Table XVI should actually be considered net forward

Table XV Special Bulk Polymer Properties in Branched Systems

IDB Branching	TDB Branching
$B_{nI,e} = \frac{\lambda_{\underline{0},\underline{\delta}_m,0}}{\lambda_{\underline{0},\underline{0},0}}$	$B_{nT} = \frac{\lambda_{\underline{0},0,1}}{\lambda_{\underline{0},\underline{0},0}}$
$B_{wI,e} = \frac{\lambda_{1,\underline{\delta}_e,0}}{\lambda_{1,0,0}} = \frac{\sum_{i=1}^{nmong} \lambda_{\underline{\delta}_i,\underline{\delta}_e,0}}{\sum_{i=1}^{nmong} \lambda_{\underline{\delta}_i,\underline{0},0}}$	$B_{wT} = \frac{\lambda_{1,0,1}}{\lambda_{1,0,0}} = \frac{\sum_{i=1}^{nmong} \lambda_{\underline{\delta}_i,\underline{0},1}}{\sum_{i=1}^{nmong} \lambda_{\underline{\delta}_i,\underline{0},0}}$

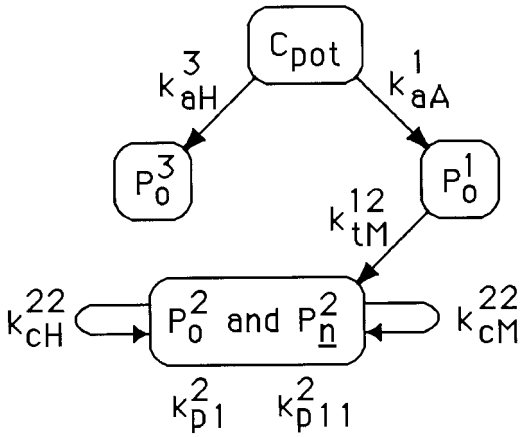

Figure 4 Example 1A: model of hydrogen rate reduction in ethylene polymerization.

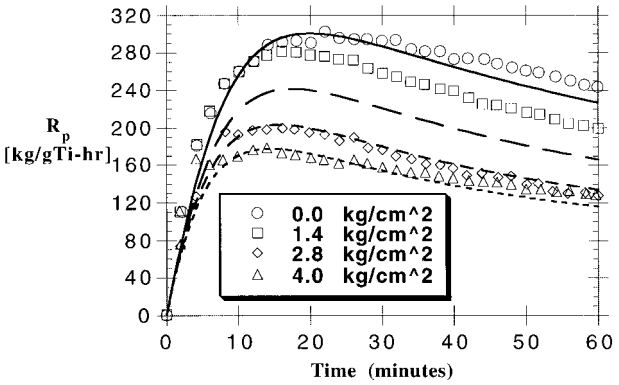

Figure 5 Example 1A: effect of hydrogen partial pressure on polymerization rate R_p.

rates. Finally, it should also be mentioned that the propagation rate constant specified for site 2 is assumed to be an average value representing propagation over a distribution of similar site types.

Figure 5 compares the rate data obtained by Kim, Kim, and Woo[27] (points) with the rate data obtained using the described model implemented in POLYRED™ (curves). As can be seen, the model matches the data fairly well in the absence of hydrogen and in the presence of high concentrations of hydrogen. At low hydrogen concentration, however, the model slightly overpredicts the rate reduction. Assuming that both the experimental data and above model are reasonable, one possible explanation for this apparent deviation could be unaccounted for hydrogen depletion reactions occurring in the bulk solution phase. In any case, the model trend and rate profiles look very promising.

As shown in Table XVII and plotted in Figure 6, agreement between the experimental and simulated number average molecular weights is very good. Applying the linear correlation originally suggested by Natta and given in eq. (2), the data are well fit using the parameters given in eq. (19).

Table XVII Example 1A: Effect of Hydrogen Partial Pressure on Molecular Weight

$P(H_2)$ [kg/cm^2]	M_n Data	M_n Simulation	M_w/M_n Data
0.0	275,200	275,410	4.52
1.4	66,200	62,300	4.84
2.8	47,400	47,796	4.87
4.0	41,500	41,328	4.76

$$M_n = (2.5 \times 10^{-6} + 1.1 \times 10^{-5}[P(\mathrm{H_2})]^{0.5})^{-1} \quad (19)$$

In closing example 1A, it should be noted that the addition of hydrogen has very little effect on the polymer's polydispersity, as shown in Table XVII. This behavior suggests that hydrogen does not act to create propagating sites which are vastly different from the sites that are active in the absence of hydrogen. However, the model must use multiple sites to predict the observed polydispersities. These are known to arise from multiple coordinating ligands and multiple oxidation states always present in these systems.

Example 1B: Polyinsertion of Propylene

As a preliminary step in studying the rate effects of hydrogen on propylene polymerizations, example 1B addresses the ability of propylene monomer to insert in more than one way. Recalling the chain transfer site regeneration theory discussed previously, the simulations in this example attempt to duplicate the experiments of Busico, Cipullo, and Corradini[11] in which hydrogen was shown to "clean" the relatively less reactive sites

Table XVI Example 1A: Simulation Parameters for Ethylene Rate Reduction by Hydrogen

Reactor Parameters:		Kinetic Parameters:	
Reactor Volume [L]	1	Activation	
Temperature [°C]	80	k^1_{aA} [L/gmol-s]	0.25
Pressure [atm]	15.05	k^3_{aH} [L/gmol-s]	0.06
Initial Conditions:		Site Transformation	
Volume [L]	0.5	k^{12}_{tM} [L/gmol-s]	18000
Hexane [gmol/L]	6.305	Initiation & Propagation	
Triethylaluminum [gmol/L]	0.0036	k^2_{p1} & k^2_{p11} [L/gmol-s]	18000
Ethylene [gmol/L]	1.013	Chain Transfer	
Hydrogen [gmol/L]	0.1022	k^{22}_{cM} [L/gmol-s]	1.83
C_{pot} [gmol/L]	6.78310^{-7}	k^{22}_{cH} [(L/gmol)$^{0.5}$-s]	54

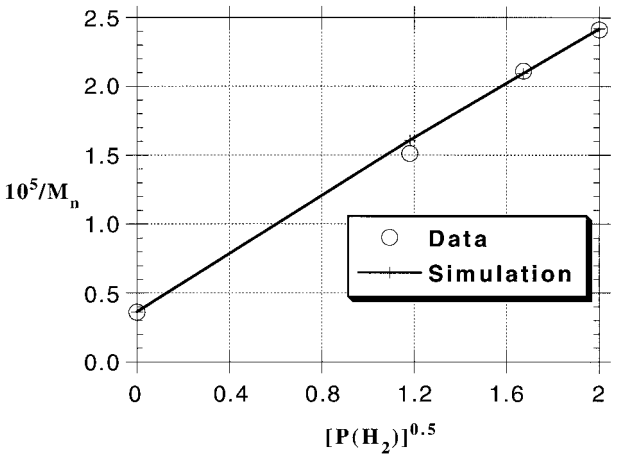

Figure 6 Example 1A: molecular weight dependence on hydrogen partial pressure.

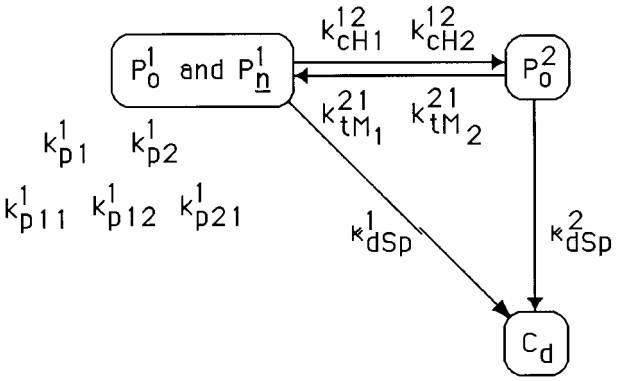

Figure 7 Example 1B: propylene polyinsertion model.

resulting from irregular 2,1-insertions. Initially the reactor contains only pentane solvent, propylene monomer, pre-activated catalyst, and 40 atm of hydrogen partial pressure. During polymerization the total pressure was then maintained constant by metering in the required amount of fresh hydrogen gas. The base case simulation parameters for isothermal operation at 50°C and 52.77 atm are given in Table XVIII.

To duplicate the kinetic scheme of Busico, Cipullo, and Corradini,[11] as shown in Figure 1, the propylene monomer is allowed two reactivities: monomer group M1 is considered to insert in the regular 1,2 mode, while monomer group M2 is assumed to insert in the irregular 2,1 fashion. Since no kinetic parameters or yield information were provided by Busico and coworkers, a value for the propagation rate constant k_{p11}^1 was taken from Kissin[18] for a typical $TiCl_4/MgCl_2$ catalyst. The remaining propagation rate constants were then calculated using the ratios suggested by Busico, Cipullo, and Corradini[11] and discussed previously.

As shown in Figure 7, the presence of hydrogen causes chain transfer from the propagating site $P_{\underline{n}}^1$ to a nonpropagating site P_0^2. This unreactive Ti-H site can then be transformed back into a propagating site via a site transformation reaction with monomer. Rate constants for chain transfer to hydrogen were assumed to be the same following either 1,2- or 2,1-insertion and the values in Table XVIII were obtained by matching the degree of polymerization for one of the data points provided by Busico and coworkers. To complete the kinetic scheme, spontaneous deactivation reactions are assumed to kill both the propagating and nonpropagating sites.

Under the current simulation conditions the fraction of growing polymer chains having irregular 2,1-inserted end groups is basically determined by the ratio of the rate constants for hydrogen chain transfer at each end group type. As shown in Figure 8 for the case of equal hydrogen chain transfer reactivity (i.e., $k_{cH1}^{12}/k_{cH2}^{12} = 1$), $\sim 10\%$ of the active sites are in a pseudo-dormant

Table XVIII Example 1B: Simulation Parameters for Propylene Polyinsertion

Reactor Parameters:		Kinetic Parameters:	
Reactor Volume [L]	2	Initiation & Propagation	
Temperature [°C]	50	k_{p1}^1 & k_{p11}^1 [L/gmol-s]	150
Pressure [atm]	52.77	k_{p2}^1 & k_{p21}^1 [L/gmol-s]	0.1364
Initial Conditions:		k_{p12}^1 [L/gmol-s]	0.6545
Volume [L]	0.4	Chain Transfer	
Pentane [gmol/L]	4.554	k_{cH1}^{12} & k_{cH2}^{12} [(L/gmol)$^{0.5}$-s]	3.07
Propylene [gmol/L]	4.81	Site Transformation	
Hydrogen [gmol/L]	0.4072	$k_{tM_1}^{21}/k_{tM_2}^{21}$ [L/gmol-s]	3/0.003
C_{pot} [gmol/L]	4.175×10^{-6}	Deactivation	
Fraction Site 1/Site 2	0.96/0.04	k_{dSp}^1/k_{dSp}^2 [L/s]	5×10^{-6}/5E $\times 10^{-8}$

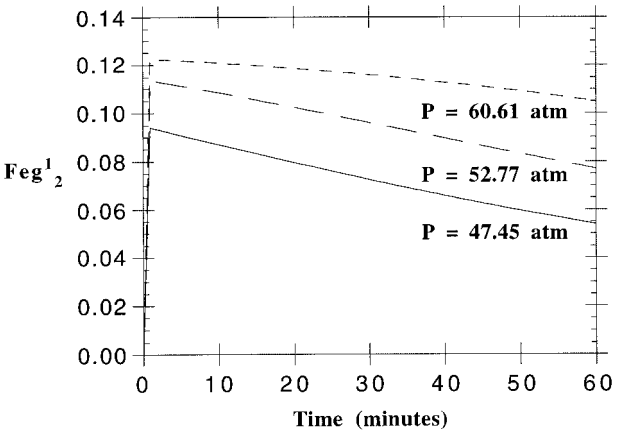

Figure 8 Example 1B: Fraction of live polymer chains having a 2,1-inserted end group as a function of total pressure.

state resulting from an irregular 2,1-insertion. This is in agreement with Busico, Cipullo, and Corradini,[11] who predicted between 10 and 30% dormancy for chain transfer reactivity ratios varying between 0.5 and 2.0. Furthermore, the fraction of irregular 2,1-inserted monomers contained in all the bulk polymer chains is of the proper order of magnitude, that is, only $\sim$ 0.1% of all monomers are reverse insertions.

In Figure 9 the ratio of 1,2-terminated chains to 2,1-terminated chains (Q_p/Q_s) is plotted versus the degree of polymerization for both Busico's experimental data and the model simulation results, including additional data points simulated at 45.0 and 64.7 atm total pressure. Although Busico and coworkers did not provide error bars for each data point, they did perform a representative error analysis for the data point at $DP_n = 320$ and obtained a value of $Q_p/Q_s = 8.4 \pm 0.4$. Thus the comparison shown in Figure 9 is very encouraging, since this very simple model is able to match the experimental results both qualitatively and quantitatively within experimental error. Based on these positive results, the next step is to actually apply this polyinsertion mechanism in a situation where the hydrogen rate enhancement is observed.

Example 1C: Hydrogen Rate Enhancement of Propylene Polymerization

Having developed the basis for propylene polyinsertion in Example 1B, it is now possible to use the same kinetic scheme to predict the hydrogen rate enhancement effect. In this example an attempt is made to duplicate a subset of the experiments of Guastalla and Giannini[8] for the polymerization of propylene over the $TiCl_4/MgCl_2/Al(Et)_3$ catalytic system in the absence and presence of hydrogen. The actual model parameters for simulation of the no-hydrogen case in a 3-L batch reactor with propylene feed for pressure control are given in Table XIX.

The simulations were initially run using the parameters from polyinsertion example 1B. Some parameters were then adjusted slightly to obtain a reasonable match to the rate enhancement obtained by Guastalla and Giannini. The only propagation rate constant changed was that for a 1,2-insertion following reverse 2,1-insertion, i.e., k^1_{p12}. This parameter was decreased from 0.6545 to 0.125 gmol/L-s. The only other parameters which needed adjusting were the rates of hydrogen chain transfer and site transformation. The hydrogen chain transfer constants were modified slightly from values of 3.07 to $k^{12}_{c\mathrm{H1}} = 4$ and $k^{12}_{c\mathrm{H2}} = 8$ $(\mathrm{L/gmol})^{0.5}$-s for transfer at 1,2- and 2,1-insertions, respectively. In choosing parameters for the site transformation by monomer from the Ti-H site back to the propagating site, it was found that using values of the corresponding propagation rate constants for each type of monomer insertion worked well, that is, $k^{21}_{tM_1} = k^1_{p11}$ and $k^{21}_{tM_2} = k^1_{p21}$.

The experimental data of Guastalla and Giannini are plotted in Figure 10, demonstrating the effect of hydrogen addition on the rate of polymerization. This is to be compared with the model simulation results plotted in Figure 11. Although systematic parameter estimation was not used to improve the data fit, the simulation results obtained are quite reasonable as compared to the

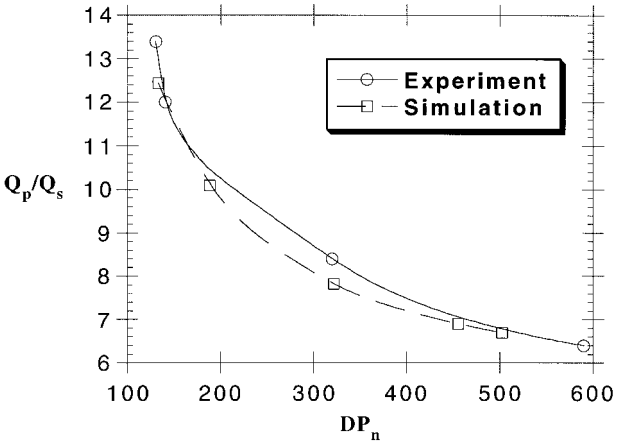

Figure 9 Example 1B: ratio of 1,2- to 2,1-terminated chains versus degree of polymerization.

Table XIX Example 1C: Simulation Parameters for Hydrogen Rate Enhancement of Propylene Polymerization

Reactor Parameters:		Kinetic Parameters:	
Reactor Volume [L]	3	Initiation & Propagation	
Temperature [°C]	70	k^1_{p1} & k^1_{p11} [L/gmol-s]	150
Pressure [atm]	3.91	k^1_{p2} & k^1_{p21} [L/gmol-s]	0.136
Initial Conditions:		k^1_{p12} [L/gmol-s]	0.125
Volume [L]	1	Chain Transfer	
Hexane [gmol/L]	6.395	$k^{12}_{cH1}/k^{12}_{cH2}$ [(L/gmol)$^{0.5}$-s]	4/8
Propylene [gmol/L]	0.8875	Site Transformation	
Hydrogen [gmol/L]	0	$k^{21}_{tM_1}/k^{21}_{tM_2}$ [L/gmol-s]	150/0.136
C_{pot} [gmol/L]	4.9164×10^{-5}	Deactivation	
Fraction Site 1/Site 2	1/0	k^1_{dSp}/k^2_{dSp} [L/s]	$5 \times 10^{-6}/5 \times 10^{-8}$

data. The model predicts the rate enhancement upon addition of 0.15 kg/cm^2 hydrogen, as well as the diminishing return obtained when the hydrogen partial pressure is doubled to 0.30 kg/cm^2. The model also shows the expected reversible behavior as the hydrogen in the reactor is used up, that is, the hydrogen-modified rate curves return asymptotically to the non-hydrogen rate curve.

Although not plotted here as in example 1B, the amount of irregular 2,1-inserted monomers which find their way into the bulk polymer chains is again slightly less than 0.1%. It is also worthwhile to consider the fraction of live polymer chains having 2,1-inserted end groups. Recalling that ~ 10% of these pseudo-dormant sites existed at high hydrogen partial pressures (example 1B), here at low hydrogen partial pressures we find ~ 52, 25, and 21% of these end groups present for 0.0, 0.15, and 0.30 kg/cm^2 hydrogen, respectively. As expected, increasing hydrogen concentration reduces the number of these pseudo-dormant sites, thus increasing the polymerization rate and resulting polymer yield.

An attempt has been made to compare the molecular weight trends predicted by the model simulations with those obtained in the actual experiments. Unfortunately, Guastalla and Giannini do not explicitly provide number or weight average molecular weight (M_w) data for the resulting polymer, rather they provide viscosity average molecular weights (M_v) for fractions in ether, heptane, and remaining residue. Assuming that M_v is approximately equal to M_w, and that the average M_w of the polymer may be calculated by summing the contribution from each weight fraction, it is possible to calculate an estimate of the polymer molecular weight. The M_w trends obtained in this way are compared with those predicted by the model in Table XX. Considering the approximate nature of the experimental M_w values, the model seems to do a reasonable job of predicting the

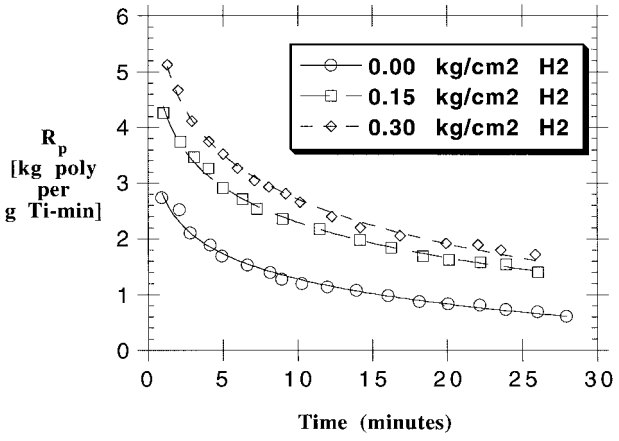

Figure 10 Example 1C: experimental rate data of Guastalla and Giannini.[8]

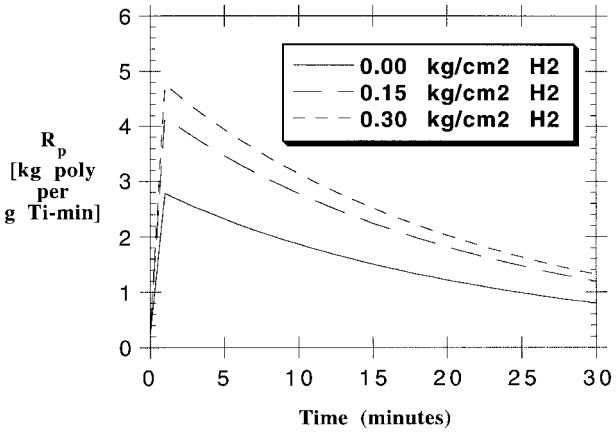

Figure 11 Example 1C: model simulation results of hydrogen rate enhancement in propylene polymerization.

Table XX Example 1C: Comparison of Weight Average Molecular Weights

$P(H_2)$ [kg/cm^2]	M_w [$=\sum w_i * M_{v,i}$]	M_w Simulation
0.00	133,000	110,000
0.15	82,000	63,000
0.30	71,000	50,400

trends in polymer molecular weight. This result is encouraging since it suggests that it is not unreasonable for the rate enhancement to be due largely to hydrogen "cleaning" of reverse 2,1-insertions.

Comonomer Rate Effects

As discussed previously, modeling comonomer rate effects can require no-death site transformations in situations where such transformations occur on the same time scales as propagation and/or chain transfer. This feature might be used, for example, to represent rapid reversible ligand coordination reactions. Although not a copolymerization, example 2A demonstrates the utility of the no-death site transformation in simulating an oscillating metallocene catalyst. Following this case study, example 2B then shows how the general Ziegler–Natta kinetics may be used to model some features of the comonomer effect, which are observed in the solution copolymerization of ethylene and 1-hexene over a $TiCl_4/MgCl_2$ catalyst.

Example 2A: Oscillating Metallocene Catalyst

It is well known that the end-use properties of polymers such as polypropylene are greatly influenced by their tacticity, the isotactic form being crystalline, and the atactic form being an amorphous gummy material. Recent work by chemists at Stanford University[29] has demonstrated the ability to control this polymer microstructure by using an oscillating metallocene catalyst that produces alternating blocks of atactic and isotactic stereosequences. The resulting elastomeric material has an advantage over conventional thermoset rubbers due to the absence of crosslinked chains which prevent recycling via melt processing.

Although other researchers have developed catalysts which can produce elastomeric polypropylene, they have been unable to modify these catalysts in a reasonable way to control the polymer microstructure. Recognizing that chiral metallocenes produce isotactic structures and achiral catalysts produce atactic structures, Waymouth and Coates[29] prepared a catalyst that oscillates between these two geometries. As shown in Figure 12, this oscillation is accomplished using an unbridged metallocene catalyst ($[2\text{-PhInd}]_2ZrCl_2$) having indenyl ligands which rotate about the metal–ligand bond. The rate of rotation is then controlled by the specific choice of substituent added to the ligand. Using the phenyl substituent shown in Figure 12, Waymouth and Coates obtain a rotation rate that is slower than the rate of monomer propagation, yet faster than the rate of chain termination. Thus an elastomeric block polypropylene is created.

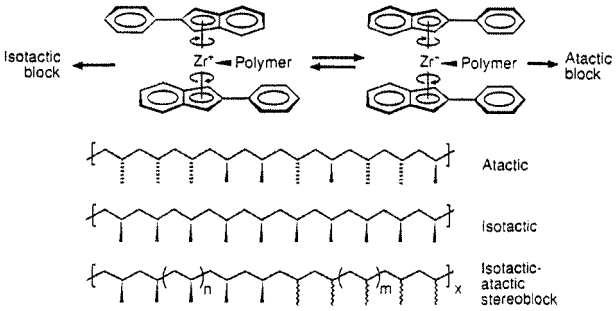

Figure 12 The oscillating metallocene catalyst $[2\text{-PhInd}]_2ZrCl_2$.[30]

As demonstrated in Figure 13, the kinetic scheme for example 2A uses no-death site transformation to simulate the formation of an atactic/isotactic block polypropylene homopolymer in a batch reactor under slurry conditions. This scheme consists of the initiation of active sites P_0^1 and P_0^2, followed by propagation, spontaneous chain transfer, spontaneous site transformation, and spontaneous deactivation. As shown in Table XXI, the initial fraction of each active site type is

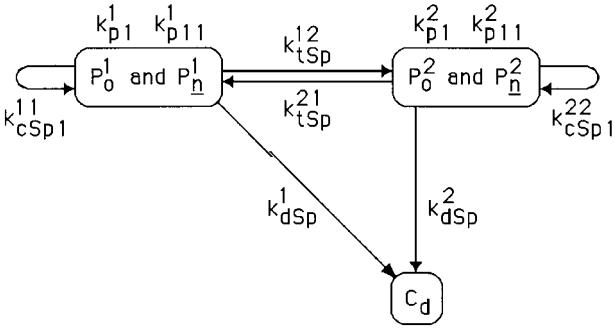

Figure 13 Example 2A: oscillating metallocene catalyst model.

Table XXI Example 2A: Simulation Parameters for Oscillating Metallocene Catalyst

Reactor Parameters:		Kinetic Parameters:	
Reactor Volume [L]	1	Monomer Effectiveness Factor	0.5
Temperature [°C]	765	Initiation & Propagation	
Pressure [atm]	20	k_{p1}^{1} & k_{p11}^{1} [L/gmol-s]	150
Initial Conditions:		k_{p1}^{2} & k_{p11}^{2} [L/gmol-s]	150
Volume [L]	0.5	Chain Transfer	
Hexane [gmol/L]	2.14	k_{cSp1}^{11} & k_{cSp1}^{22} [L/s]	0.45
Propylene [gmol/L]	7.47	Site Transformation	
C_{pot} [gmol/L]	4.175×10^{-7}	k_{tSp}^{12} & k_{tSp}^{21} [L/s]	0.0001
Fraction Site 1/Site 2	0.5/0.5	Deactivation	
Tacticity Site 1/Site 2	0.98/0.00	k_{dSp}^{1}/k_{dSp}^{2} [L/s]	$5 \times 10^{-6}/5 \times 10^{-6}$

0.5 and both sites have the same kinetic behavior. The only difference between the sites is that $P_{\underline{n}}^{1}$ produces 98% isotactic polymer, while $P_{\underline{n}}^{2}$ produces atactic polymer. As indicated by the specific isothermal temperature and constant pressure being simulated, the reactor is considered to be operating under slurry conditions. With this in mind, the effectiveness factor of the propylene monomer has been set to 0.5 to account for the fact that sorption and diffusion will significantly reduce the effective monomer concentration at the catalyst active sites.

The result of running the above simulation with the standard site transformation kinetics is demonstrated in Figure 14. When the rate constant for spontaneous site transformation is zero or several orders of magnitude less than the rate constant for spontaneous chain transfer (e.g., 0.0001 and 0.01), little or no effect is observed in the number average degree of polymerization DP_n. As the rate of site transformation increases

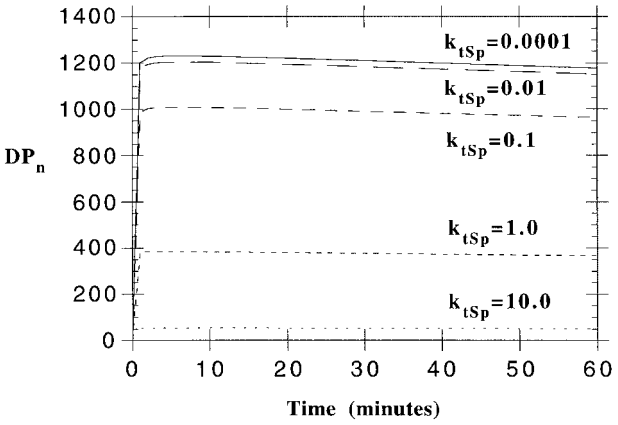

Figure 14 The effect of spontaneous site transformation rate on the number average degree of polymerization.

to the same order of magnitude and higher (e.g., 0.1, 1, and 10), however, the degree of polymerization drops significantly due to the model's requirement that dead polymer be formed after each transformation. Such behavior is clearly unsatisfactory for simulating the case of the oscillating catalyst discussed above, hence no-death site transformations must be utilized. When this is done, the original DP_n of $\sim$ 1200 is recovered, regardless of the rate of any site transformation reactions.

Continuing to use no-death site transformation, the base case model needs to be modified slightly in order to simulate the production of an isotactic/atactic block polymer. The main change is the requirement that propylene be given two reactive monomer groups. By allowing the first monomer group M1 to polymerize only at the isotactic site $P_{\underline{n}}^{1}$, and the second monomer group M2 to polymerize only at the atactic site $P_{\underline{n}}^{2}$, it will be possible to calculate the sequence lengths of each monomer group. When this modification is made and the rate constants are adjusted to account for the presence of the additional monomer group/end group, one obtains the same bulk polymer properties as the initial base case, as well as the desired sequence length information shown in Figure 15.

In Figure 15 one sees the effect of varying the rate of site transformation from $P_{\underline{n}}^{1}$ (isotactic) to $P_{\underline{n}}^{2}$ (atactic), while maintaining the rate of the reverse site transformation reaction constant ($k_{tSp}^{21} = 10$). As expected, halving the transformation rate doubles the isotactic sequence length to $\sim$ 100 monomer units, and doubling the rate halves the isotactic sequence length to $\sim$ 25 monomer units. The corresponding change in the composite polymer tacticity is shown in Figure 16. These data demonstrate that the resulting degree

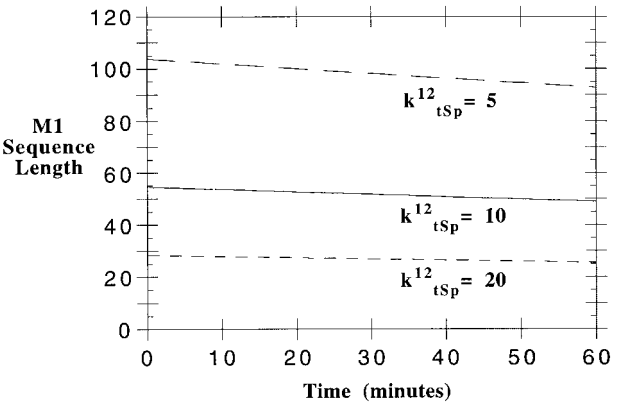

Figure 15 The effect of spontaneous site transformation rate on the sequence length of monomer 1 (isotactic propylene).

of tacticity under the current simulation conditions depends only on the ratio of the forward to the reverse site transformation.

Example 2B: Ethylene/1-Hexene Copolymerization

In this example the comonomer rate effect is investigated for the solution copolymerization of ethylene and 1-hexene over a $TiCl_4/MgCl_2$ catalyst. The data provided in the work of Jaber and Ray[31] has been used as the basis for this example, since it provides the most detail in terms of the reaction system and conditions used. Furthermore, under the high temperature solution conditions employed, any observed rate effects are more likely due to chemical factors rather than physical ones (e.g., diffusion).

Jaber and Ray used a 1-L reactor operating at constant pressure via the metered inlet flow of

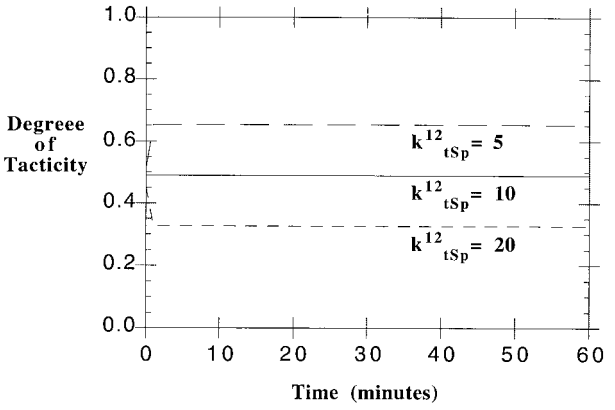

Figure 16 Tacticity resulting from changes in the rate of spontaneous site transformation from site 1 to site 2.

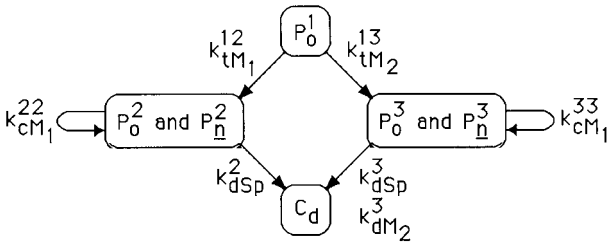

Figure 17 Example 2B: ethylene/1-hexene copolymerization model (initiation and propagation rate constants not shown).

ethylene. Although not shown here, their results clearly show a rate increase and corresponding accelerated decay upon addition of 1-hexene comonomer to the polymerization of ethylene.

In attempting to model this observed comonomer effect, the following approach was taken. First, a simple model was suggested for the homopolymerization case. Next, the model's parameters were adjusted to match the observed rate, yield, and degree of polymerization. Starting from this base simulation for homopolymerization, the model was then expanded to handle copolymerization. While maintaining consistency with the homopolymerization results, the parameters of the expanded model were then used to match the observed rate, yield, degree of polymerization, and comonomer incorporation for the 1-hexene copolymerization.

The simple model which resulted from the above process is shown schematically in Figure 17. According to this model there is a pre-activated catalyst site P^1_0, which must be modified by ethylene or 1-hexene before any polymerization can occur. Thus only an ethylene modified site P^2_0 will be available for homopolymerization and an additional 1-hexene site P^3_0 will be present during copolymerization. As evidenced in data of Jaber and Ray, a fast decay is present in all polymerizations under the high temperature conditions. For this reason a spontaneous deactivation is assumed to be occurring at both the ethylene P^2_0 and 1-hexene P^3_0-type sites. This may be thought of as resulting from a rapid reduction in the catalyst oxidation state at such high temperatures.

Due to the greater concentration and fast reactivity of ethylene, the molecular weight is assumed to be controlled primarily by ethylene. Hence the ethylene chain transfer constants at the polymerizing sites have been adjusted to yield the observed number average degree of polymer-

Table XXII Example 2B: Comonomer Effect Simulation Parameters

Reactor Parameters:		Kinetic Parameters:	
Reactor Volume [L]	1	Initiation & Propagation	
Temperature [°C]	185	[L/gmol-s]	
Pressure [psig]	400	$k_{p1}^2, k_{p1}^3, k_{p11}^2, k_{p11}^3, k_{p12}^2, k_{p12}^3$	11000
Initial Conditions:		$k_{p2}^2, k_{p2}^3, k_{p21}^2, k_{p21}^3, k_{p22}^2, k_{p22}^3$	308
Volume [L]	0.4	Chain Transfer	
Isopar-E [gmol/L]	4.5	$k_{cM_1}^{22}/k_{cM_1}^{33}$ [L/gmol-s]	12.6/7
Ethylene [gmol/L]	0.83	Site Transformation	
1-Hexene [gmol/L]	0.27	$k_{tM_1}^{12}/k_{tM_2}^{13}$ [L/gmol-s]	150/0.136
Hydrogen [gmol/L]	0	Deactivation	
C_{pot} [gmol/L]	8.76×10^{-7}	k_{dSp}^2 & $k_{dSp}^3/k_{dM_2}^3$ [L/s]	0.0068/0.04

ization. In a similar fashion, the propagation constant for 1-hexene was adjusted to provide the correct comonomer incorporation. Finally, to account for the accelerated deactivation in the presence of comonomer, the 1-hexene modified site (site 3) is also assumed to be deactivated by the comonomer itself. Such deactivation is consistent with the bis-vacant model of Karol discussed earlier. However, these data could also be explained by the rapid oxidation state change of Ti, where Ti^{+2} will not copolymerize.

The actual simulation parameters are summarized in Table XXII and a comparison of the simulation results with the experimental results is provided in Figure 18. The corresponding yields, maximum polymerization rates, number average degrees of polymerization, and percent comonomer incorporation are given in Table XXIII.

Despite some scatter in the experimental data, the simulation does a reasonable job of matching the curves with the very simple model proposed. Although it is frequently suggested that the rate enhancement is due to increased numbers of sites and/or the formation of more reactive sites in the presence of comonomer, the above model accomplishes a rate enhancement by maintaining the same number of sites, each having the same propagation rate. The more significant factors in the current simulation are the rates at which active sites are formed and the rates at which these sites decay. One possible explanation for this behavior is that, under such high temperature conditions, polymerization rates are very large at both site types so that any differences become less significant relative to site deactivation. Thus the system becomes dominated by catalyst decay dynamics.

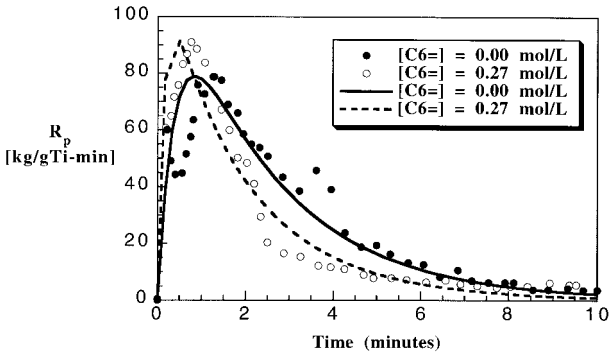

Figure 18 Comparison of simulation (lines) and experimental (points) rates of polymerization R_p.

Long Chain Branching

In the final example we consider the addition of long chain branches via the terminal double bond mechanism discussed earlier. Although there is no detailed literature or industrial data with which to compare results directly, example 3 is designed to be similar in respect to Dow Chemical's metallocene catalyzed solution polymerization process. For an example, using the internal double bond polymerization mechanism, the reader is referred to the thesis of Han-Adebekun[24] where the production of EPDM is modeled for the solution process.

Example 3: Terminal Double Bond Polymerization

This example considers the continuous isothermal solution homopolymerization of ethylene in a continuous stirred tank reactor (CSTR). A simple single site model is used to simulate a metallocene catalyst which is capable of adding branches via the TDB mechanism. The reactor is initially filled with Isopar-E solvent, ethylene monomer, and activated catalyst. No gas phase is considered, thus polymerization is sustained by the incoming flow of fresh solvent, monomer, and activated catalyst. The specific reactor and kinetic parameters used

Table XXIII Comparison of Simulation and Experimental Results

	Experiment				Simulation			
$[C_6]$ mol/L	Yield kg/gTi	$R_{p,\max}$ kg/gTi-min	M_n	C_6 mol %	Yield kg/gTi	$R_{p,\max}$ kg/gTi-min	M_n	C_6 mol %
0.00	259	78	21,700	0.00	263	79	21,800	0.00
0.27	217	92	29,900	0.53	219	93	29,800	0.53

in the simulation are given in Table XXIV. Estimated values of the initiation and propagation rate constants were taken from Kissin,[18] and the rate constant for branch addition was assumed to be of the same order of magnitude due to the similarity of the reaction. Kissin was also the source for the initial estimates of the rate constants for chain transfer and deactivation; however, these values were then modified slightly as required to agree with other literature data on physical properties such as polymer molecular weight and terminal double bond unsaturation obtained under similar high-temperature solution conditions.

As evidenced from the parameters in Table XXIV, the kinetic scheme for these simulations includes initiation by monomer, propagation, hydrogen chain transfer to form saturated dead polymer, monomer chain transfer to form unreacted terminal double bonds, TDB branch formation, and spontaneous site deactivation. It should be noted that since the TDB branching reaction is being used, there is one more live end group in addition to the ethylene end group. This reacted TDB ($rtdb$) end group allows one to vary the site reactivity following branch addition. Furthermore, yet a third end group type is needed to track the number of dead polymer chains having unsaturated end groups.

In all the simulations of this section, chain transfer was only allowed at end group 1 (ethylene) and not at end group 2 ($rtdb$). Chain transfer following chain addition was not considered simply because the number of live chains having the $rtdb$ end group (0.01%) is insignificant relative to those having the ethylene end group. Since there is no polymer in the reactor at startup ($t = 0$), there is an initial transient period during which the active catalyst sites are initiated for propagation and the concentration of unreacted terminal double bonds is established. In the graphs which follow, several parameters have been varied to observe the effect on the resulting steady state bulk polymer properties.

The first parameter considered was the reactor temperature. As demonstrated in Table XXV, however, varying this parameter simultaneously modifies the concentrations of ethylene and hydrogen due to their changing solubilities. Due to the lack of data for branching metallocene catalyst systems, the data of Jaber and Ray[32] for the $TiCl_4/MgCl_2/AlEt_3$ has been used as the basis for both the kinetic and solubility data required by this example. As taken from this paper, the data in Table XXV show that the concentration of ethylene decreases and the concentration of hydrogen increases as the reactor temperature is increased. Also included in this table is an estimate of the

Table XXIV Example 3: TDB Polymerization Simulation Parameters

Reactor Parameters:		Kinetic Parameters:	
Reactor Volume [L]	5000	Initiation & Propagation	
Temperature [°C]	170	k^1_{p1}, k^1_{p11}, k^1_{p12} [L/gmol-s]	10,000
Feed Rate [L/s]	16.667	E^1_{p1}/E^1_{p11}, E^1_{p12} [kcal/mol]	5/10
End Group 1	Ethylene	TDB Branch Formation	
End Group 2	TDB Branch	k^1_{TDB31}/E^1_{TDB31}	10,000/10
End Group 3	Unsaturated	Chain Transfer	
Initial Conditions:		k^{11}_{cH1} [(L/gmol)$^{0.5}$/s]/E^{11}_{cH1} [kcal/mol]	20/10
Volume [L]	5000	Unsaturation Formation	
Isopar-E [gmol/L]	5	$k^{11}_{uM_11}$ [L/gmol-s]/$E^{11}_{uM_11}$ [kcal/mol]	6.3/10
Ethylene/Hydrogen [gmol/L]	0.72/0.0045	Deactivation	
C_{pot} [gmol/L]	9×10^{-7}	k^1_{dSp} [L/s]/E^1_{dSp} [kcal/mol]	0.005/20

Table XXV Effect of Temperature on Ethylene and Hydrogen Concentrations in Isopar-E

Temperature (°C)	Ethylene (gmol/L)	Hydrogen (gmol/L)	Experimental DP_n	Simulation DP_n
150	0.84	0.0040	1960	1954
170	0.72	0.0045	1710	1722
190	0.61	0.0049	1500	1547

resulting temperature effect on the number average degree of polymerization obtained using the above-mentioned titanium catalyst system. These values, extrapolated from the data of Jaber and Ray, provided reasonable points with which to tie down the chain transfer rate constants for monomer and hydrogen.

Of course, to observe the effects of varying temperature, it was also necessary to obtain reasonable estimates for the activation energies of all the corresponding reactions used in the simulation. For the propagation reactions, sources suggest numbers varying between 5 and 15 kcal/mol, hence a value of 10 kcal/mol has been assumed to be a reasonable estimate over the 150–190°C temperature range considered here. Furthermore, since the branching reaction is itself just the propagation of a unit having a very long hydrocarbon tail, the value of 10 kcal/mol was also assumed reasonable for branch addition.

With regard to the initiation reaction, a value of 5 kcal/mol was used since it seems reasonable that the activation energy should be less than that for propagation since there is no metal–carbon bond being broken. For chain transfer to both hydrogen and monomer it was assumed that the activation energy was again dominated by the breaking of a carbon–metal bond, hence the 10 kcal/mol estimate was applied yet again. Finally, due to the known sensitivity of catalyst deactivation to increasing temperature, a value of 20 kcal/mol was assumed for this spontaneous reaction.

As mentioned previously, the rate constants for hydrogen and monomer chain transfer were adjusted to provide molecular weights which were consistent with the data of Jaber and Ray in Table XXV. In addition, however, the relative rates of hydrogen chain transfer to form terminal saturated bonds and monomer chain transfer to form terminal unsaturated bonds had to satisfy the requirement that the fraction of unsaturated terminal double bonds was near 50%. Based on the experimental results of Kashiwa, Tsutsui, and Toyota[33] for the solution polymerization of ethylene in hexane at 170°C, this additional requirement also influenced the rate constants which were finally selected and presented in Table XXIV with the other simulation parameters.

The resulting fraction of unsaturated terminal double bonds and number average degrees of polymerization at 150, 170, and 190°C are shown in Figures 19 and 20, respectively. As expected, increasing temperature results in increased rates of chain transfer which lead to decreasing molecular weights. The resulting steady-state number average degrees of polymerization for the POLYRED™ simulations are also provided in Table XXV for comparison with the data of Jaber and Ray. Less expected, however, is the predicted minimum in the fraction of chains having unsaturated end groups (*Futdb*). The apparent minimum in *Futdb* between 150 and 190°C is probably a balance between the activation energies chosen as well as the half-order dependence on hydrogen in the hydrogen chain transfer reaction. In particular, the increasingly important effect of catalyst deactivation at higher temperatures is certainly involved. Whether or not such a minimum in *Futdb* actually occurs in practice is too difficult to

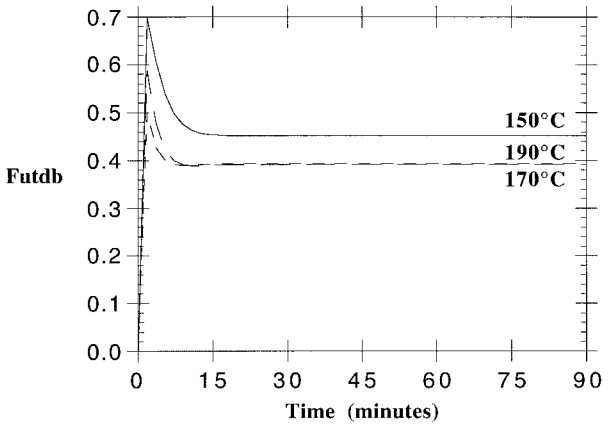

Figure 19 Effect of reaction temperature on the fraction of bulk polymer chains having unreacted terminal double bonds (Futdb).

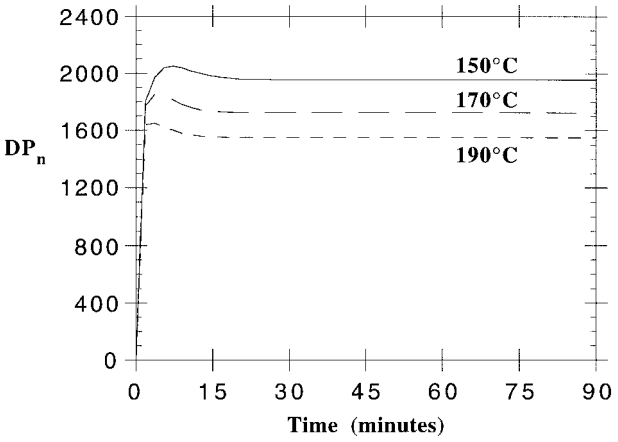

Figure 20 Effect of reaction temperature on the number average degree of polymerization.

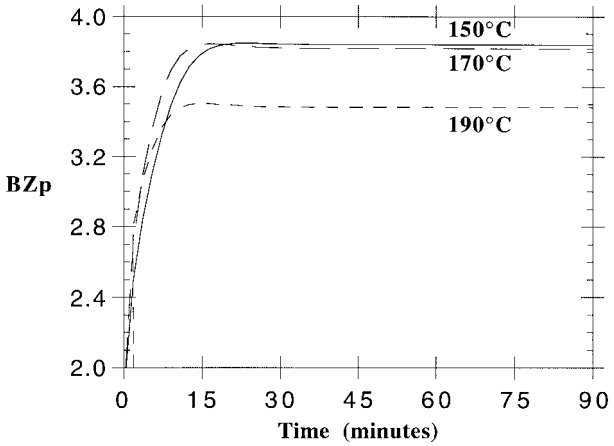

Figure 22 Effect of reaction temperature on branching polydispersity.

predict without the benefit of accurate data on such unsaturated systems.

It is now worthwhile to consider the special properties of the polymer which results from using the TDB branching reaction. The number average degrees of branching (B_{nT}), i.e., the average number of branches per polymer chain, are shown in Figure 21 at each simulated reactor temperature. As one might expect based on the earlier plot showing the fraction of unsaturated terminal double bonds (*Futdb*) versus temperature, the largest number of branches per chain is obtained at 150°C. Unlike the *Futdb*, however, the degree of branching decreases monotonically over the simulated temperature range.

In discussing the branching data shown in Figure 21, it is also interesting to consider the fact that increasing the reactor temperature simultaneously produces shorter chain lengths. Calculating the average number of branch points per repeat unit by dividing B_{nT} by D_{Pn}, one obtains 0.000293, 0.000297, and 0.000271 at 150, 170, and 190°C, respectively. Thus the number of branches per unit length of chain is actually observed to go through a maximum under the current simulation conditions.

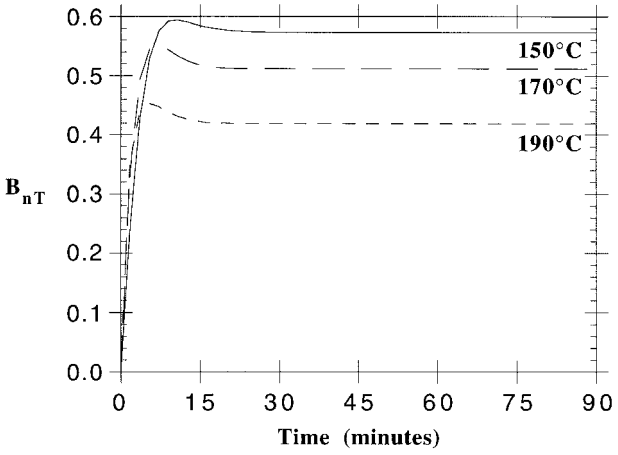

Figure 21 Effect of reaction temperature on number average degree of branching.

Figure 22 shows the branching polydispersity (BZ_p), i.e., uniformity of branch distribution, obtained by dividing the weight average degree of branching (B_{wT}) by B_{nT}. Although the distribution of branches broadens with increased branching as expected, it is initially curious why the values at 150 and 170°C should be so close. Considering the discussion in the previous paragraph, however, this behavior is very likely due to the fact that although B_{nT} is significantly larger at 150°C, the average number of branch points per repeat unit is greater at 170°C.

To round out the discussion of the effects of temperature on the branched polymerization considered here, graphs showing the bulk polymer polydispersity and reactor yield in kg/g catalyst are presented in Figures 23 and 24. The decrease in polydispersity with increasing temperature is due to the corresponding decrease in the number of branches per polymer chain. In the case of the polymer yield, despite the increasing propagation rate with increasing temperature, the dominating effect here is the large activation energy for deactivation which causes significant decreases in productivity with increasing temperature.

Of course, there are many other parameters which can be varied to effect a change in the resulting polymer properties. A few of the parame-

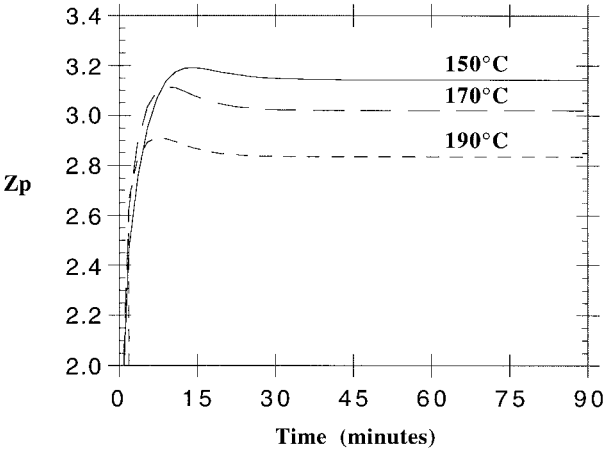

Figure 23 Effect of temperature on bulk polymer polydispersity.

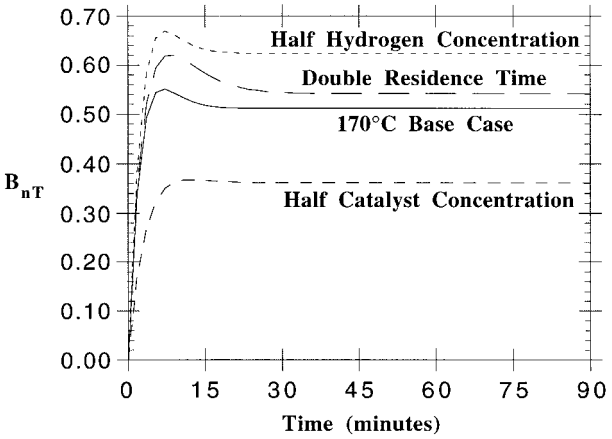

Figure 25 Effects of varying hydrogen concentration, reactor residence time, and catalyst concentration on the number average degree of branching.

ters affecting the number average degree of branching, for example, have been investigated and are shown in Figure 25. Starting from the previous 170°C base case presented in Table XXIV, one can see the effect of doubling the reactor residence time from 5 to 10 min by cutting the reactor inlet flow in half. The resulting small increase in the number of branches per chain is simply a consequence of having a higher steady-state concentration of dead polymer chains which can react to form branches. A more significant increase in B_{nT} may be obtained by reducing the hydrogen concentration. As shown in Figure 25, this effectively increases the number of branches by reducing the rate of chain transfer with hydrogen to form chains with saturated ends. Finally, much like changing the residence time, adjusting the catalyst concentration can significantly affect the available concentration of dead polymer chains available in the reactor to form branches. As demonstrated, reducing the catalyst concentration by a factor of two drops B_{nT} from about one branch on every other chain to about one branch on every third chain.

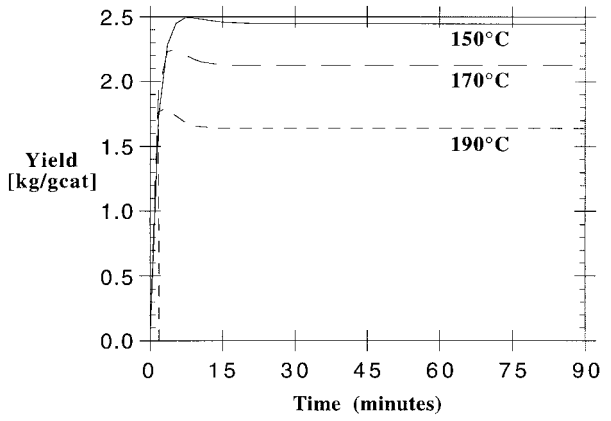

Figure 24 Effect of temperature on reactor productivity.

SUMMARY

This paper has focused on modeling several poorly understood phenomena which are known to occur in catalyzed olefin polymerizations. Significant extensions to models currently available in the literature have been made, including the following:

Hydrogen Rate Effects

- Allows multiple insertion mechanisms for each monomer
- Permits simultaneous chain transfer/site transformation reactions

Comonomer Rate Effects

- Adopts the concept of reversible ligand coordination via no-death site transformations
- Allows one to model trigger propagation and/or deactivation
- Incorporates a simple parameter for specifying propagation order for matching experimental data when the mechanism is unknown

Long Chain Branching

- Introduces reactions required to create terminal unsaturation
- Includes reactions to describe both IDB and TDB branch addition reactions

In each of the examples provided, the general kinetic model has been applied to a continuous or batch-operated stirred tank solution polymerization reactor with the sole purpose of demonstrating the model's capabilities. Although the specific models presented in each example were necessarily simple due to the fact that parameter estimation has not been applied, they may provide a useful starting point for future comparisons with more comprehensive data sets. All of the examples presented here were calculated using the POLYRED™ simulation package.[2]

REFERENCES

1. C. M. Chen, Ph.D. Thesis, University of Wisconsin-Madison, 1993.
2. I. Hyanek, J. Zacca, F. Teymour, and W. H. Ray, *Ind. Eng. Chem. Res.,* **34,** 3872 (1995).
3. G. Natta, G. Mazzanti, P. Longi, and F. Bernadini, *Chim. Ind.* (*Milan*), **41,** 519 (1959).
4. A. S. Hoffman, B. A. Fries, and P. C. Condit, *J. Polym. Sci. C,* **4,** 109 (1963).
5. G. Bourat, J. Ferrier, and A. Perez, *J. Polym. Sci. C,* **4,** 103 (1963).
6. C. D. Mason and R. J. Schaffhauser, *J. Polym. Sci. B,* **9,** 661 (1971).
7. I. Okura, K. Soga, A. Kojima, and T. Keii, *J. Polym. Sci. A,* **8,** 2717 (1970).
8. G. Guastalla and U. Giannini, *Makromol. Chem. Rapid Commun.,* **4,** 519 (1983).
9. B. Boucheron, *Eur. Polym. J.,* **11,** 131 (1975).
10. E. M. Pijpers and B. C. Foest, *Eur. Polym. J.,* **8,** 1151 (1972).
11. V. Busico, R. Cipullo, and P. Corradini, *Makromol. Chem. Rapid Commun.,* **13,** 15 (1992).
12. T. Tsutsui, N. Kashiwa, and A. Mizuno, *Makromol. Chem. Rapid Commun.,* **11,** 565 (1990).
13. J. C. Chadwick, A. Miedema, and O. Sudmeijer, *Macromol. Chem. Phys.,* **195,** 167 (1994).
14. I. W. Parsons and T. M. Al-Turki, *Polym. Commun.,* **30,** 720 (1989).
15. A. Valvassori, G. Sartori, G. Mazzanti, and G. Pajaro, *Makromol. Chem.,* **61,** 46 (1963).
16. S. S. Ivanchev, A. V. Kryzhanovskii, I. I. Gapon, and Y. L. Ponomareva, *Polym. Sci. USSR,* **32,** 64 (1990).
17. F. J. Karol, S.-C. Kao, and K. J. Cann, *J. Polym. Sci. A,* **31,** 2541 (1993).
18. Y. V. Kissin, *J. Molec. Catal.,* **56,** 220 (1989).
19. A. Yamamoto, *Organotransition Metal Chemistry,* Wiley-Interscience, New York, 1986.
20. M. Brookhart and D. M. Lincoln, *J. Am. Chem. Soc.,* **110,** 8719 (1988).
21. M. Ystenes, *J. Catal.,* **129,** 383 (1991).
22. L. Resconi, F. Piemontesi, G. Franciscono, L. Abis, and T. Fiorani, *J. Am. Chem. Soc.,* **114,** 1025 (1992).
23. J. C. W. Chien and D. He, *J. Polym. Sci. A,* **29,** 1585 (1991).
24. G. C. Han-Adebekun, Ph.D. Thesis, University of Wisconsin-Madison, 1996.
25. D. J. Arriola, Ph.D. Thesis, University of Wisconsin-Madison, 1989.
26. W. K. A. Shaffer, M.S. Thesis, University of Wisconsin-Madison, 1995.
27. I. L. Kim, J. H. Kim, and S. I. Woo, *J. Appl. Polym. Sci.,* **39,** 837 (1990).
28. R. A. Hutchinson, Ph.D. Thesis, University of Wisconsin-Madison, 1990.
29. R. M. Waymouth and G. W. Coates, *Science,* **267,** 222 (1995).
30. R. Baum, *Chem. Eng. News,* **1,** 6 (1995).
31. I. A. Jaber and W. H. Ray, *J. Appl. Polym. Sci.,* **49,** 1709 (1993).
32. I. A. Jaber and W. H. Ray, *J. Appl. Polym. Sci.,* **50,** 201 (1993).
33. N. Kashiwa, T. Tsutsui, and A. Toyota, *Polym. Bull.,* **12,** 111 (1984).